Self-healing Construction Materials

Polymer Microcapsules Using Microfluidics

by

Liam Carter (SE)

Fourth-year undergraduate project in
Group D, 2014/2015

I hereby declare that, except where specifically indicated, the work submitted herein is my own original work.

Signed: _____ Date: _____

Technical Abstract

Self-healing Construction Materials

Polymer Microcapsules Using Microfluidics

Liam Carter (SE)

Group D

2014/15

Concrete dominates the construction industry due to its versatility and price. Current production exceeds 10 billion tons a year, and the demand for concrete continues to increase. The concrete industry contributes around 7% of global CO_2 emissions and this will grow with increased demand. Concrete, therefore, represents an area where a small increase in sustainability could have a big impact.

The brittle nature of concrete leads to the use of steel reinforcement in tensile regions. The steel is highly susceptible to corrosion due to chloride ion ingress, which is increased in the presence of cracks. Degradation of the reinforcing steel can be detrimental to the integrity of concrete structures and is one of the leading causes of structure failure. Expensive maintenance is used to repair cracks and increase a structures lifespan, however, it is impractical in many structures.

Self-healing concrete aims to remove the need for maintenance, by engineering concrete with the ability to respond to damage. A healing agent is contained within the structure and released into cracks as they form, leading to decreased chloride ion ingress and regain of mechanical strength. A range of delivery mechanisms and healing agents are currently being investigated. Self-healing concrete has the potential to offer increased structure lifespan and hence, improve the concrete industry sustainability. Additionally, safety improvements are expected, particularly in inaccessible structures such as those offshore.

Within this report the literature on self-healing concrete and microfluidics is reviewed. Two forms of self-healing were found to dominate the literature, vascular networks and microcapsules. Various methods of microcapule production had been tried, however, microcapsules produced using microfluidic techniques were found to have not been used in self-healing concrete, presenting an untried research area. Literature on microcapsule based self-healing also called for capsules which are flexible during mixing but become brittle once set.

Dynamic Mechanical Analysis was used to determine the thermo-mechanical properties of UV curable acrylate polymers, known to have been used to produce microcapsules using microfluidics. A material which, due to its glass transition temperature, became flexible and tough upon heating to 50^{o}C, but once cooled to 20^{o}C became brittle, was found by

forming a copolymer of the acrylates tested. Pre-heating of the microcapsules made from this material, before mixing, would place them in their tough ductile state. During mixing the exothermic cement hydration reaction would maintain capsules in their tough state increasing survivability during the mix.

The chosen shell material solution was then used in a commercially purchased microfluidic chip to produce microcapsules. Due to time considerations some deviations from the selected material were made to ease production of microcapsules and enable further tests to be conducted. Using the new shell material solution, the effect of microfluidic flow rates on produced double emulsion droplets was determined, enabling fine size control of the produced droplets.

Polymerising the droplets to form microcapsules with solid polymer shells and liquid cores was conducted using a UV lamp. The polymerisation resulted in a non uniform shell wall thickness. A capillary pressure, established while drying, led to buckling of the capsules, in some cases resulting in fracture. Improvements were made to the process resulting in a higher yield, however, further improvements are still required. Capsules were observed and characterised using optical and scanning electron microscopy and the yield calculated using thermogravimetric analysis.

Capsules were cast in small cement prisms to view their behaviour in a fracture plane. The method described in the literature for assessing survivability of capsules during mixing was deemed unsatisfactory and alternatives were proposed. Upon fracture of freshly demoulded samples, capsules were seen to pull out of the matrix rather than fracture, indicating poor bond strength with the cement matrix. Continued hydration of samples for 3 days gave improved results, the liquid core of the capsules was observed to have flown from damaged capsules using SEM. However, capsule fracture only appeared to occur due to crushing under compressive load and bonding was still not sufficiently strong to inhibit pull out in tensile loading.

In conclusion, it was shown that microfluidically produced microcapsules could be cast in cement paste and capsule fracture, leading to core material release, observed under compressive loading. Demonstration of capsule fracture and core material release shows the potential for a self-healing mechanism, should a healing agent be encapsulated. However, to be truly successfully in a self healing context, fracture of the capsules is required under tensile loading. This requires that the bond strength between the capsules and cement matrix is increased. Possible methods of achieving this, as well as other key work required to make this a feasible self-healing mechanism, are presented.

Contents

1 Introduction and Motivation

Concrete is the most widely used construction material in the world, with production exceeding 10 billion tons a year and contributing to about 7% of global CO_2 emissions [Meyer, 2004]. Clearly any improvement to the sustainability of concrete production or structures will have a significant impact.

Concrete displays excellent compressive properties. However, addition of steel reinforcement is required to carry tension. Chloride induced corrosion of the reinforcing steel is the primary cause of degradation in reinforced concrete structures, particularly those situated in corrosive offshore environments [Val and Stewart, 2003]. Chloride ingress into structures is increased when cracks are present, these typically form in tensile regions. Maintenance is carried out on concrete structures to repair cracks and extend the life span. Maintenance is estimated to be 45% of the total construction costs in the UK [Woudhuysen, 2004]. Self-healing concrete aims to repair cracks arising in concrete without the need for human intervention, reducing maintenance costs, and offering safety improvements, particularly in inaccessible structures where maintenance is not possible.

The material cost of self-healing concrete is expected to exceed traditional concretes. However, the lifetime cost of a self-healing structure should be less than a traditional structure undergoing repairs, as shown in Figure 1. Reduced need for maintenance and extended lifespan of structures will be beneficial, both economically and environmentally, in the ever growing concrete market.

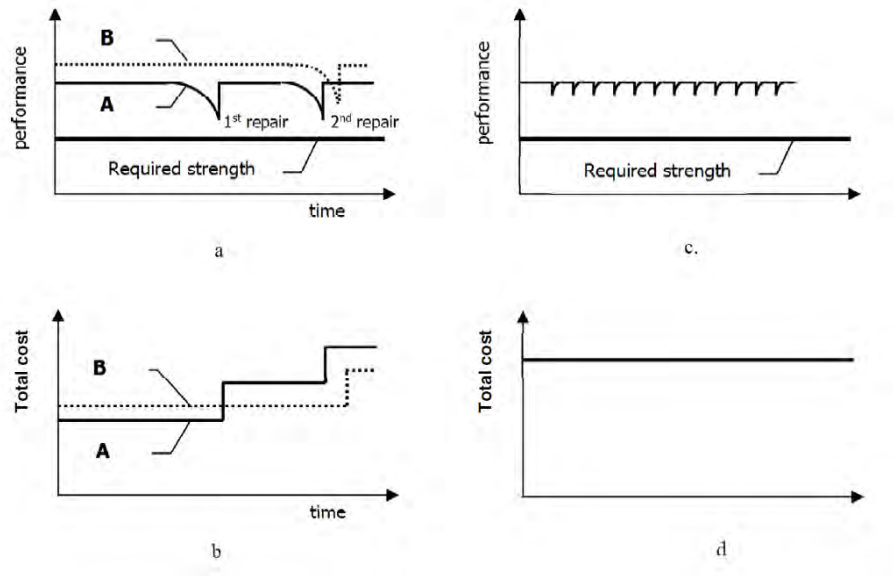

Figure 1: a) The performance over time of a standard (A) and high performance (B) concrete structure. b) The resulting total cost for a standard and high performance structure. c) Performance for a self-healing structure. d) Total cost for a self-healing structure. [De Rooij and Schlangen, 2011].

2 Literature Review

2.1 Self-healing in Cementitious Materials

While man-made engineering materials can exceed the stiffness or strength of biological materials, they lack the ability to repair themselves. Ongoing research is investigating ways of facilitating self-healing in man-made materials, taking inspiration from biology. The following section will summarise some of the key literature relating to the field of self-healing construction materials with particular emphasis on microcapsule based mechanisms.

2.1.1 Introduction to Self-healing

Self-healing can be broadly defined into two types: autogenic and autonomic, [De Rooij and Schlangen, 2011]. Autogenic healing utilises components typically present in the material matrix, i.e. not included for a self-healing purpose, for the healing process. Autonomic healing applies to materials in which specific additives have been included to facilitate healing.

Cementitious materials are an excellent example of autogenic healing materials. Two main mechanisms are proposed for the healing: hydration of unhydrated regions of cement or dissolution and carbonation of $Ca(OH)_2$. Since cementitious materials can self-heal, what is the rational for investigating autonomic forms of self-healing? Well the limitations of autogenic self-healing are substantial. Firstly, the maximum crack size autogenic self-healing can seal is relatively small, reports vary between 5 and 300 μm, [Van Tittelboom and De Belie, 2013]. Secondly, it is most effective in concretes with a low water : binder ratio which is unfavourable economically and environmentally, [Van der Zwaag, 2010]. Both mechanisms require water ingress which may be limited and is hard to control. Various strategies have been employed to improve autogeneous healing. Inclusion of PVA fibres in the matrix encourages the formation of many micro-cracks instead of a single large crack, facilitating improved autogenic healing [Yang et al., 2011].

Autonomic healing has the potential to offer greater self healing capabilities. Delivery of a healing agent to the crack generally occurs after release from either a microcapsule or a vascular network. Vascular networks consist of an interconnected series of tubes placed in the concrete matrix. The healing agent can be released either actively or passively. In the simplest passive case, fracture of the cement matrix leads to fracture of a brittle tube and release of the healing agent into the crack. Active modes require human intervention to facilitate healing, for example Dry [1994a] investigated active methods; the first of which is based on the passive mode, however, healing agent is pumped through the tube,

allowing for multiple healing events and a greater agent supply. Active methods offer more control, however, the complexity of the systems will be difficult to scale up.

Microcapsules with a solid shell, diameter on the order of 100 μm, and liquid core are dispersed throughout the concrete matrix. They will typically target smaller cracks than vascular networks, but act in a more localised manner. Healing agent is released from the microcapsules due to fracture of the capsules or by a chemical trigger. Provided microcapsules can be made to survive the mixing process, they offer a distinct advantage over vascular networks as they can be directly incorporated into the mix. Vascular networks however, must be pre-placed in the mould and the cement cast around them, increasing handling difficulties.

Vascular networks designed to ensure that the healing agent only cures in the crack, while remaining fluid in the tubing, offer the ability to heal multiple times in the same location. Microcapsules however, can only heal a location once. If a second crack appears in the same location, the capsules are already depleted. This disadvantage could be negated by using an adhesive with a higher tensile modulus than concrete, as subsequent cracks will be more likely to form in the weaker surrounding concrete regions [Van Tittelboom and De Belie, 2013].

2.1.2 Microcapsule based Self-healing

The released healing agent from a microcapsule can typically lead to crack closure in three ways. The first is a reaction with either air, water or the cement matrix. Agents have included adhesives such 1 part epoxys, or solutions of sodium silicate which react with the cement matrix to form CSH, a cement hydration product [Van Tittelboom and De Belie, 2013].

Secondly, the healing agent may react with catalyst particles dispersed throughout the cement matrix. Kaltzakorta et al. [2013] utilised this method, producing silica shelled capsules with an epoxy core. The epoxy hardened by catalysis with amine nano particles included in the cement. They also noted the favourable interaction between cement paste and the silica shell giving good adhesion.

Finally, a two component agent released from separate capsules which sets upon mixing. Mihashi et al. [2001] pursued this method but encountered difficulties in achieving sufficient mixing of the 2 part epoxy used.

When selecting a healing agent, several important considerations need to be made. As the crack may be wet, this should not hinder the agents ability to cure [Van Tittelboom and De Belie, 2013]. The viscosity of the healing agent should be considered, too low and

the agent will leak from the crack into the surrounding matrix, too high and flow from the capsule will be inhibited. Dry [1994b] stated the ideal viscosity range is 100-500 cPs. However, as shown by Joseph et al. [2010] cyanoacrylate (<10 cPs) is an effective agent, due to its fast curing time preventing significant leakage from the crack.

Capsules are required to survive the mixing process, however, the capsules must also fracture in the cement matrix. Dry [1994b] recommends research investigating capsules which, during mixing are ductile and tough, but become brittle once the matrix has set. Inspired by this Hilloulin et al. [2015] utilised the exothermic cement hydration reaction to achieve this in larger cylindrical capsules, 5 cm long. They constructed capsules from polymers which were brittle at room temperature. Before mixing they preheated the capsules. Heating increased the mobility of the polymeric chains, increasing the ductility and fracture toughness during mixing. The exothermic cement hydration reaction maintained the capsules at an elevated temperature during mixing. They showed this increased the survivability of the capsules during the mixing process. After mixing, the temperature decreased and the polymer capsules returned to their glassy brittle state. For this method to work the polymer shell needs a suitable glass transition temperature (T_g).

Additional essential requirements of the capsule shell are:

- Low permeability - To contain the healing agent and prevent early curing.
- Resistance to alkaline cement environment.
- Bond strength with cement matrix - The bond strength must be higher than the capsule strength to ensure capsule fracture occurs rather than pull out.

2.2 Microfluidics

Microfluidics offers a method of microcapsule production which is as yet untried in the field of self-healing construction materials. This section of the literature review will introduce some of the fundamentals of microfluidics with a focus on its use for microcapsule production.

2.2.1 Principles of Microfluidics

Microfluidics is a rapidly growing field involving the manipulation of fluids through channels on the micron scale. Microfluidics' uses span a wide range of areas with particular interest in the pharmaceutical and chemical industries [Squires and Quake, 2005].

The small channel size leads to a small Reynolds number (Re), which is the ratio of inertial to viscous force:

$$Re = \frac{\rho U L}{\mu} \tag{1}$$

where ρ is the density, U the characteristic velocity, L the characteristic length and μ the dynamic viscosity. Re is typically 10^{-6} to 10^{1} in microfluidic channels. At small Re viscous forces dominate inertial forces giving rise to laminar, Stokes flow with little to no turbulence, hence mixing of fluids only occurs by diffusion.

Due to the large surface area to volume ratio, surface forces become considerable. They are a key factor in enabling the formation of droplets. Surface forces result in a second dimensionless number, the capillary number (Ca) which relates viscous forces to surface forces.

$$Ca = \frac{\mu U}{\gamma} \tag{2}$$

where γ is the surface tension.

2.2.2 Microcapsule Production

Microfluidics can be used to create droplets when two immiscible fluids flow together. The simplest channel arrangement is the T junction. However, more commonly used, particularly when extending to double emulsion droplets, is the flow focuser shown in Figure 2.

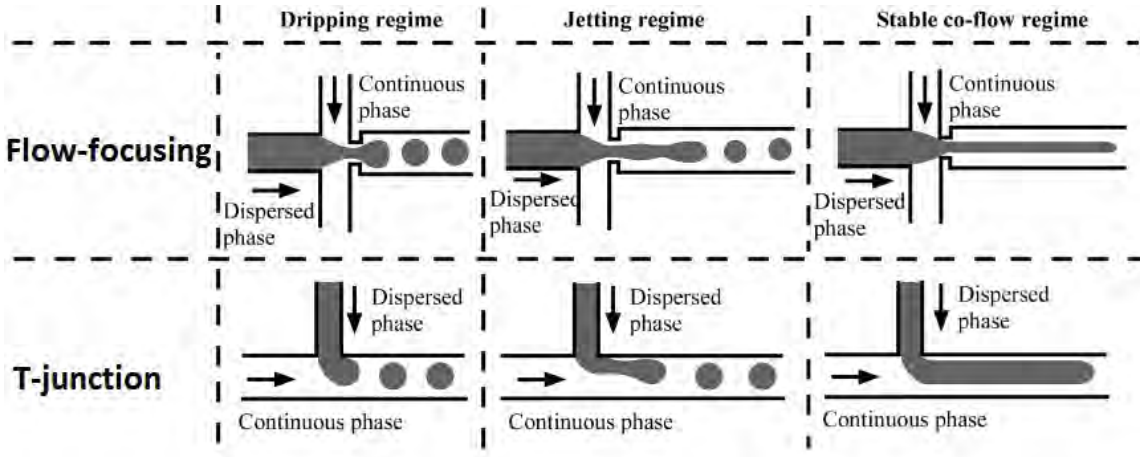

Figure 2: Channel geometry and flow conditions for droplet generation. Adapted from [Nunes et al., 2013].

In a flow-focusing device, droplet formation occurs in two regimens, dripping or jetting. In dripping, droplets of the disperse fluid form in the continuous fluid at the channel junction. The continuous fluid shears the disperse fluid, generating a neck in the junction. Surface forces then act to minimise the surface area of the neck, facilitating breakup and droplet formation. As the continuous phase velocity increases, viscous forces increase relative to surface forces, increasing Ca. This results in extension of the neck, forming jet travelling downstream of the junction, marking the transition to jetting, [Cramer et al., 2004]. The jet undergoes breakup by the Rayleigh-Plateau instability, again a surface force driven process. In the jetting regime, 'satellite' of 'secondary' droplets often form due to the breakup dynamics [Cramer et al., 2004]. The phases used in the continuous and disperse channels determine the types of emulsion produced. An oil disperse phase with a water continuous phase will produce an oil in water (O/W) emulsion and vice versa will give a W/O emulsion.

Surfactants, which reduce interfacial surface tension, can be added to change the breakup dynamics. Small amounts of surfactant facilitate droplet breakup, due to perturbations formed in the neck [Hu et al., 2000], and prevent coalescence of formed droplets [Peng et al., 2011]. Large amounts of surfactant, that reduce surface tension to $< 10^{-1}$ mN/m, inhibit break up as surface forces become negligible, hence a stable co-flow regime is reached, Figure 2, [Nunes et al., 2013].

By extending the droplet generation idea to produce a droplet within a droplet, a double emulsion, the formation of microcapsules is possible. This can be achieved by placing two flow-focusing junctions in series, Figure 3.

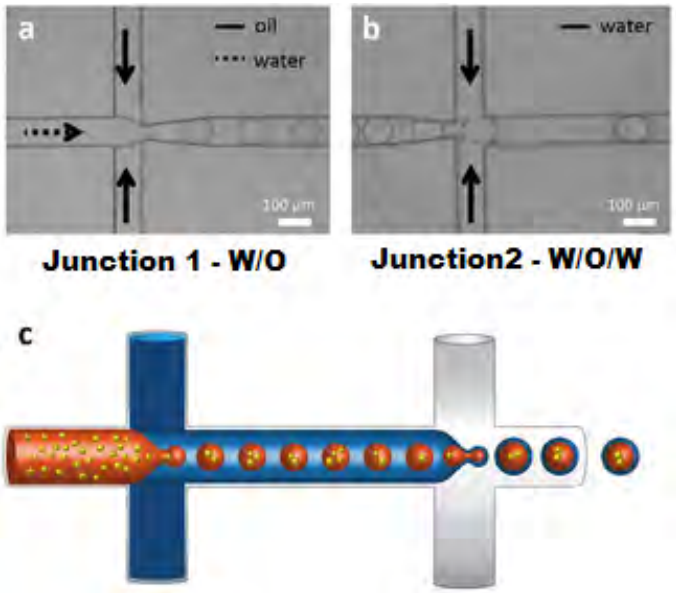

Figure 3: Microfluidic chip for production of double emulsions (W/O/W). a) Generation of first emulsion W/O. b) Generation of second emulsion surrounding first W/O/W. c) Overall chip geometry. Adapted from [Chan et al., 2013].

Alternatively, both emulsions can be formed in a single junction, such as the capillary system used by Chen et al. [2011]. Using this system, Chen was able to produce double emulsions with varying internal and outer diameters by varying the flow rates of the inner, middle and outer fluids, Figure 4A.

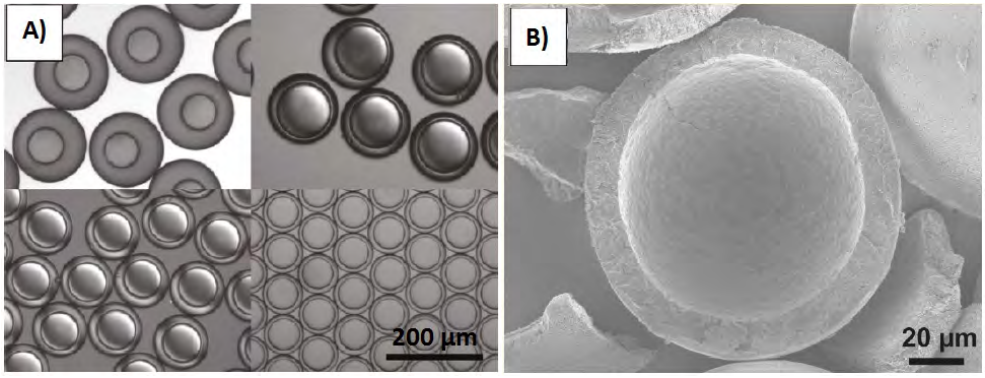

Figure 4: A) Varied double emulsion droplets. B) Broken microcapsule formed after polymerisation. Adapted from [Chen et al., 2011].

Larger variation in droplet size was achieved by varying the channel size. Nunes et al. [2013] and Nie et al. [2005] also report similar behaviour, however, no universal analytical model predicting the size of a droplet has, to present, been developed.

Production of a microcapsule from a double emulsion requires the solidification of the middle phase, forming a solid shell. Chen utilised a UV curable acrylate monomer, which forms a polymer shell upon UV exposure, Figure 4B. Chen also produced capsules with varying mechanical properties, by using a monomer solution consisting of different acrylates. A 100% Isoborynl acrylate (IBOA) shell produced a brittle shell, whereas a 1:1 mix of IBOA and 2-phenoxyethyl acrylate (PEA) produced ductile capsules. This is due to the difference in T_g of PEA (5^oC) and IBOA (52^oC). Alternative polymerisation methods include initiation of a cross linking reaction in a heated water bath forming a silicon rubber shell [Vilanova et al., 2013].

The advantages of microcapsules produced using microfluidics over more traditional methods are: the precise control of dimensions and the monodispersity of the produced capsules, the low level of mixing between core and shell materials due to laminar flow conditions and the variety of possible shell and core combinations available.

2.3 Aims and Objectives

During this project, the focus will be on investigating whether acrylate polymer microcapsules produced using microfluidics are a viable means of achieving self-healing behaviour in cementitious materials. Due to acrylate polymers resistance to alkaline environments [Athawale and Kulkarni, 2009], they meet the requirement set out previously. They can also be made with a low permeability, however, the acrylate-cement bond strength is an unknown factor which will need investigating. Additionally, the methodology applied by Hilloulin et al. [2015] to larger polymer capsules to increase the survivability will be investigated in microcapules. This will require using a polymer shell with a suitable glass transition temperature. Due to the behaviour of IBOA and PEA, shown by Chen, these will be suitable starting points.

The aims of the project are to:

- Determine the thermo-mechanical properties of the acrylate polymers to be used in the microcapsule shell.
- Identify a shell material capable of undergoing a temperature dependant ductile-brittle change. Allowing capsules to be ductile during mixing and brittle once set, Figure 5.

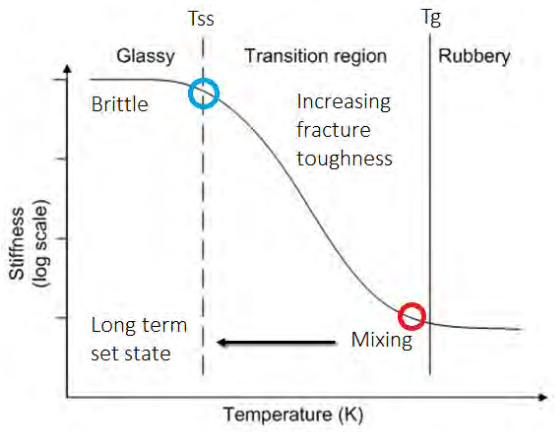

Figure 5: Proposed capsule behaviour during mixing. T_g is the glass transition temperature and T_{ss} is the long term set state temperature for the capsule in the matrix. Capsules are heated to the region highlighted in red and then placed in the mix. After mixing they cool and follow the same curve back to the region highlighted in blue, regaining brittleness.

- Produce microcapsules using microfluidics and quantify the effect of flow rates on capsule size and thickness.
- Analyse the behaviour of capsules during mixing, casting and fracture of construction materials.

3 Apparatus and Methodology

In this section the apparatus and experimental methodology used during the study will be described. Details of why the technique was used and how the experiments were carried out will be provided.

3.1 Polymer Prism Production

Polymerisation of acrylates occurs when free radicals react with the acrylate double bond, enabling the formation of a polymeric chain. The free radicals are generated when a photoinitiator (Darocur 1173) absorbs photons of UV light. Making samples for DMA testing, therefore, requires a UV permeable mould. Samples were required to be approximately 30 x 10 x 3 mm. Samples were produced using a transparency sheet open top box, with the desired sample dimensions, Figure 6.

Figure 6: Transparency sheet box used with a top sheet to produce sample. Sample also shown.

Constructed by scoring a box net onto the transparency, cutting, folding into shape and securing with tape. The monomer solution was injected into the box, a rectangle of transparency sheet was placed on top to prevent oxygen inhibition. It was necessary to fill the box until a convex meniscus developed, to prevent air bubbles forming. The sample was polymerised for 300s using a Sylvania BL350 UV lamp. Monomer solutions were produced by calculating the volume of each material required and pipetting the required amount into a conical bottom tube wrapped in aluminium foil to prevent polymerisation.

3.2 Dynamic Mechanical Analysis

Dynamic mechanical analysis (DMA) measures the visco-elastic and temperature dependant properties of materials. Conducting the DMA tests has three main purposes. The first is to establish the optimum photoinitiator concentration for achieving fast polymerisation. The second is to establish modulus values for the polymers to help to understand the behaviour of the capsules. Finally, to establish the glass transition temperature (T_g) of the polymers. While some data was found in the literature, it was inconsistent, particularly with regard to T_g. For example, stated values for IBOA were 52^{o}C [Chen et al., 2011] and 88^{o}C [Glöckner, 2008]. Testing was conducted using a Triton Technology Dynamic Mechanical Analyser in its single cantilever configuration, Figure 7.

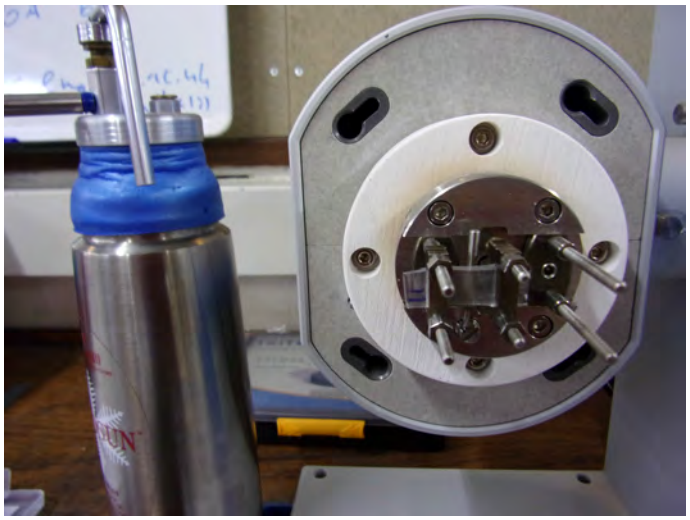

Figure 7: Sample mounted in the DMA single cantilever configuration with the climate chamber removed.

Required sample dimensions were 30 x 10 mm with a thickness of 3mm.

A temperature scan of the elastic and loss modulus was run for the samples, in the following manner: 1) The sample thickness and width were measured at 4 locations and averaged. 2) The sample was placed between the clamps and tightened evenly using a torque wrench. 3) The length between the clamps was measured and the sample dimensions input into the DMA software. 4) The desired ending temperature was entered along with a ramp rate of 3 ^{o}C/min, sampling interval of 3 s, test frequency of 1 Hz and displacement of 0.02 mm. 5) If required, the sample was cooled to a specified temperature using liquid nitrogen. The glass transition temperature was then found from the peak of the tan(δ) curve, where δ is the phase angle between the elastic and loss modulus.

3.3 Microfluidics

All droplets were produced using a microfluidic double emulsion chip, Figure 8, purchased from Dolomite Microfluidics. This systems is designed for use with pressure pumps, however, for this study Graseby^{TM} 3150 syringe pumps were used due to their immediate availability in the department.

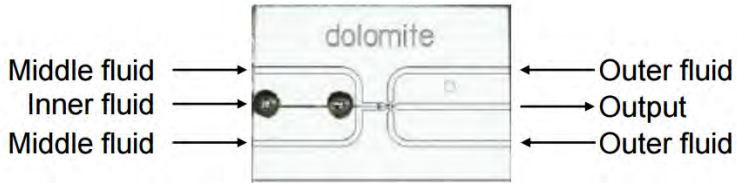

Figure 8: Channel layout of the microfluidic chip used showing inputs and outputs, [Dolomite Microfluidics, 2010].

Initial experiments were conducted as follows: 1) Syringes were filled with the inner, middle and outer fluids. Inner and outer fluid (water phases) were 2 wt% PVA solution. PVA is used as a surfactant and additionally provides steric hindrance between droplets preventing coalescence [Lankveld and Lyklema, 1972]. The middle fluid (oil phase) is the optimal copolymer solution found from DMA testing. 2) Syringes were connected to the microfluidic chip via tubing. 3) Volumetric flow rates were controlled using the syringe pumps seen in Figure 9, typical ranges were: outer 30-130 μl/min, middle 10-35 μl/min, inner 1-6 μl/min.

As the project progressed, pressure pumps were purchased, slightly altering the methods. The revised set-up is shown in Figure 10.

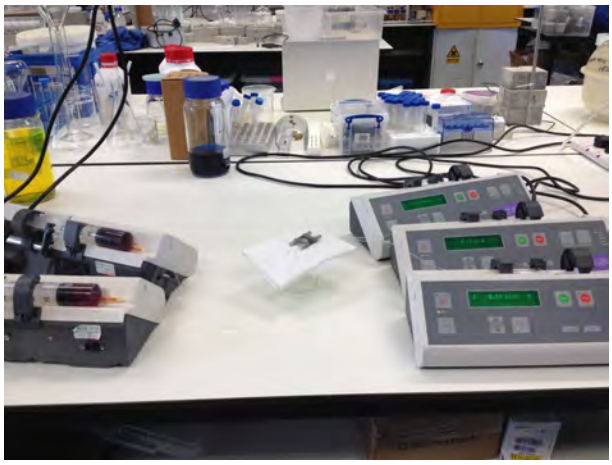

Figure 9: Set-up using syringe pumps.

Figure 10: Set-up using 3 pressure pumps.

All subsequent tests were conducted with pressure pump's as follows: 1) Solutions were placed in glass vials in the relevant pumps pressure chamber. 2) Pump pressure specified using the supplied software, ranges used shown in appendix A.2. 3) Once droplets began

forming, two of the three flows (inner, middle and outer) were switched to flow control, maintaining a fixed flow rate. 4) The pressure, and hence flow rate, of the third fluid was varied. 5) Once the flow rate stabilised, observed using the software, droplets were collected and observed using a Leica DM 2700M microscope. 6) The images were analysed using ImageJ, the internal and outer diameter were measured and recorded together with the flow rates and pressures.

3.4 Microcapsule Production

To form microcapsules, the double emulsions are polymerised by UV exposure. Droplets were collected in a UV permeable petri-dish and placed above the Sylvania BL350 UV lamp. A foil reflector was placed above to achieve more even polymerisation. Oxygen inhibition is negated due to submerged polymerisation [Studer et al., 2003]. Polymerised capsules were filtered and washed twice with distilled water to remove PVA from the outer solution and stored underwater in glass vials.

3.5 Thermogravimetric Analysis

Thermogravimetric analysis calculates the mass loss of a sample with increasing temperature enabling the water content of the capsules to be found. Before testing, capsules were dried under vacuum for 48 hours, therefore, it can be assumed that any water loss must come from water contained within the capsule.

Procedure: 1) A crucible is placed in the measuring chamber and the system tared. 2) Capsules are placed into the crucible (around 4 mg). 3) A temperature range of 40 - 750^{o}C with a ramp rate of 5^{o}C/min specified. 4) Data collected and the sample mass percent plotted against the temperature. The test is repeated using a sample of the capsule shell material.

3.6 Cement Paste Prisms

Cement paste prisms, size 10 x 10 x 100 mm, were formed using CEM_I 52.5 cement in proportions of 45g water per 100g cement powder, Figure 11. Capsules were included at 3.4 wt%, typical of the amount used in literature, Wang et al. [2013] used 3-9 wt% and Wang et al. [2014] 1-5 wt%.

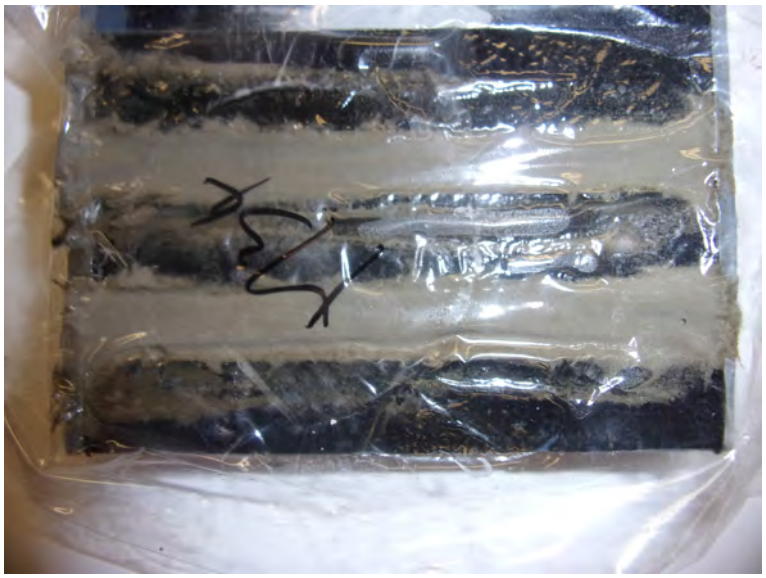

Figure 11: Mould used for casting cement paste prisms. 2 prisms curing.

Procedure: 1) The mould was brushed with oil to aid de-moulding. 2) Cement powder, capsules and water were weighed out. 3) Capsules were dispersed in half the water and the other half was added to the cement powder and mixed with a pallet knife. 4) The dispersed capsules were added and mixed until homogeneous. 5) The cement paste was poured into the mould, placed on a vibrating table to remove air bubbles, coated with a polymer film and left to cure for 24 hours. 6) Samples were de-moulded and labelled. 7) Half the samples were placed underwater, the other half were broken immediately. Samples were broken by hand bending and then a hammer and chisel used to shape to appropriate lengths for SEM imaging before being placed under vacuum for 48 hours to dry.

4 Results and Discussion

In this section, the results from experiments conducted during the project will be presented and discussed. They will be compared to theory and any results presented in the literature. Additionally, initial experimentation results used to refine methods will be discussed.

4.1 Polymer Prism Production

Before the method detailed in section 3.1 was used for production, several other methods were tried. Initially using an uncovered transparency sheet box was tried, with the monomer exposed to UV for 300s. The top surface remained liquid while the lower material polymerised, further UV exposure did not increase the proportion cured. This was due to oxygen inhibition. Oxygen inhibition occurs when the free radicals generated by the photoinitiator react with oxygen present at the surface, inhibiting polymerisation [Studer et al., 2003].

To successfully cure uniform samples, it is necessary that no surfaces are exposed to oxygen. A method similar to that used by López-García et al. [2007] was tried. This method used a glass slide, onto which a piece of transparency sheet was adhered using a drop of water. An aluminium sheet of the sample thickness was placed on top and the monomer solution injected into slots cut in this sheet. This was covered with another transparency coated glass slide and exposed to UV light. This achieved complete polymerisation of the sample, however, the polymer bound to the aluminium sheet, preventing removal. To prevent the sample binding, the transparency sheet on the UV light side was printed with a mask designed to prevent polymerisation close to the metal, Figure 12. However, diffraction of light still resulted in binding to the metal. These experiments led to the final method as detailed in section 3.1.

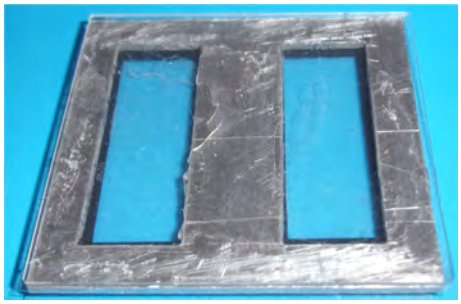

Figure 12: The aluminium sheet method for producing polymer samples, including the mask to prevent adhesion to the metal.

4.2 Dynamic Mechanical Analysis

4.2.1 Initial Testing

Initial tests were conducted using a ramp rate of 7.5^{o}C/min. When conducting tests with PEA, which required cooling to -50^{o}C with liquid nitrogen, due to is low glass transition temperature, the results did not follow the characteristic modulus-temperature curve typical of polymers. The test ended with the climate chamber at 20^{o}C, on removal of the sample it felt colder than expected, suggesting heat transfer to the sample was a limiting factor. Reducing the sample thickness to 2mm and the ramp rate to 3 ^{o}C/min was found to prevent this problem.

For each new material tested, a trial run was conducted using a wide temperature range, based on literature or previous data, the results were plotted in real time and the experiment terminated a few degrees after T_g was observed. This data provided the temperature range used for subsequent tests.

4.2.2 Individual Polymers

Achieving a uniform, fast cure will be important in achieving successful polymerisation of the microcapsules. Low levels of photoinitator will not completely cure samples, leaving un-reacted monomer which may be removed from the shell, increasing porosity. Too much photoinitator causes most of the UV to be absorbed in the surface, achieving complete cure of the surface but reduced cure in the bulk, a particular issue for thick samples [Wicks et al., 2007]. Both IBOA and PEA were tested with varying photoinitator concentration and the modulus at a temperature in the glassy plateau was measured, Figure 13.

Both cases showed that 2 wt% photoinitator gave the highest modulus and is, therefore, assumed to give the best cure and will be used in subsequent testing. Due to IBOA being brittle at room temperature, tightening clamps to the torque wrench limit would often fracture the sample. For IBOA the clamps had to be left slightly looser, thus resulting in greater result spread than the error bars would predict.

The modulus of IBOA found in the literature was 210 MPa [López-García et al., 2007]. This is 5.5 times smaller than the value measured in this experiment of 1.17 GPa showing that the short polymerisation times used by Lopez of 10-13.5 s are not sufficient to fully cure the samples. Lopez also noted a decrease in modulus in 1 day old samples, this was not noticed during experimentation with several samples retested after 1 week with no significant change. Additionally the T_g found for IBOA during this project was 110^{o}C, higher than the values found in the literature. This discrepancy may be caused by variations in the monomer supplier or the polymerisation conditions. Tests on PEA also

produced similar results with the measured T_g of 22^{o}C being higher than the published values of -22^{o}C and 5^{o}C.

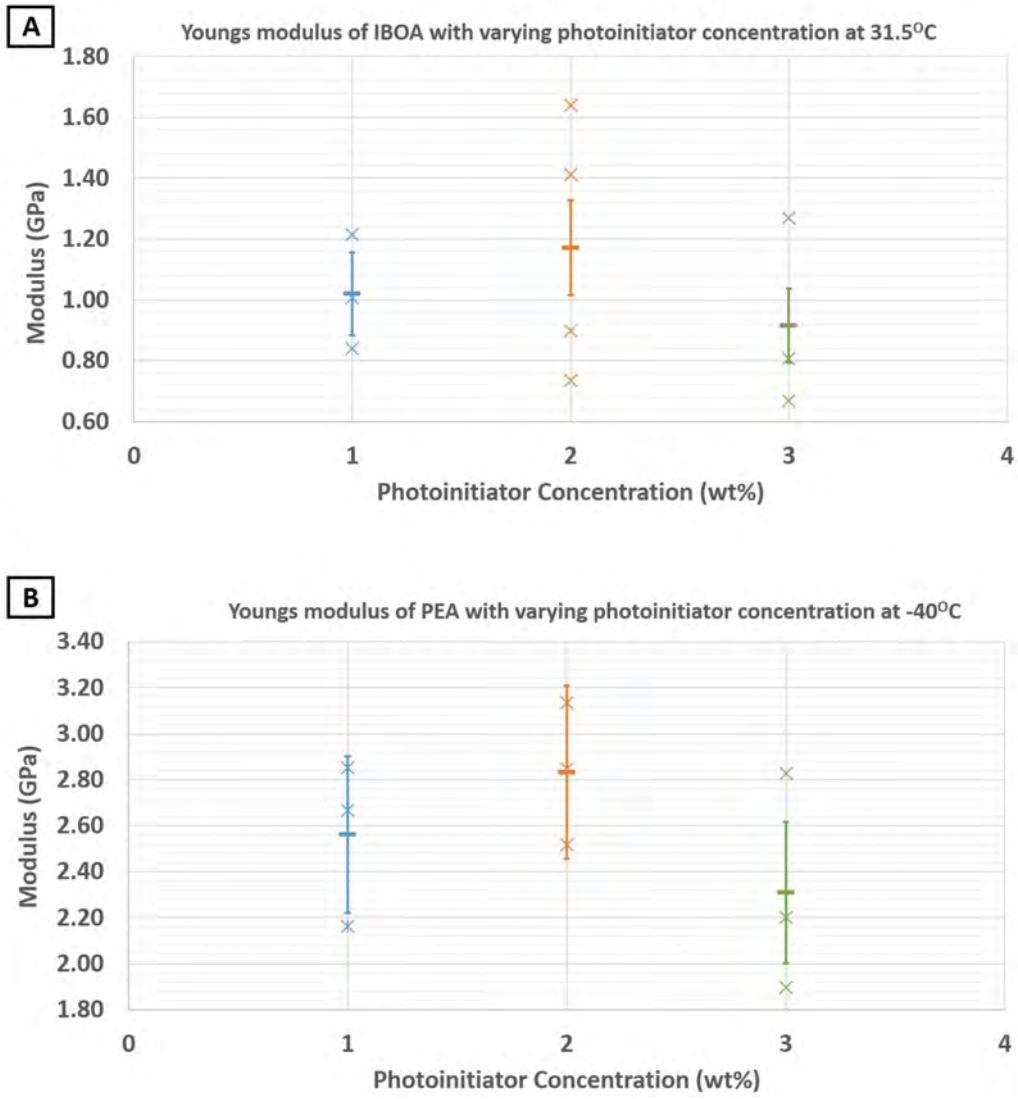

Figure 13: The Youngs modulus of IBOA (A) and PEA (B) in their glassy regions with varying amounts of photoinitiator. Error bars are centred around the mean and represent the propagated error in measuring the sample dimensions.

4.2.3 Copolymers

Finding a shell material with the desired glass transition temperature, required mixing IBOA and PEA to form a copolymer. The Fox equation is commonly used to predict the glass transition temperature of a copolymer, it is given by [Fox, 1956]:

$$\frac{1}{T_g} = \frac{w_1}{T_{g,1}} + \frac{w_2}{T_{g,2}} \tag{3}$$

.

where w_1 and w_2 are the weight fractions of each polymer and $T_{g,1}$ and $T_{g,2}$ the glass transition temperatures in Kelvin. Often copolymers will deviate from the Fox Law due to structural factors which arise due to the chain arrangement [Lee and Litt, 2000], however the Fox Law still provides a guide to start investigations. Initially a T_g of 70^{o}C was aimed for suggesting a 60 wt% IBOA solution.

A deviation was made from the Fox Law as at least 1 wt% HDDA was added. This is a cross linker which decreases the porosity of the polymer, an important factor for microcapsules. Chen et al. [2011] found 0.5 wt% HDDA decreased core leakage to 0%. A minimum of 1 wt% was, therefore, expected to be used in the microcapsules and hence, also the samples tested here. The addition of crosslinkers is expected to increase T_g due to reduced chain mobility [Chattopadhyay et al., 2005], however, at the very small quantity used, the effect is expected to be negligible. Figure 14 shows the measured T_g compared to the predicted.

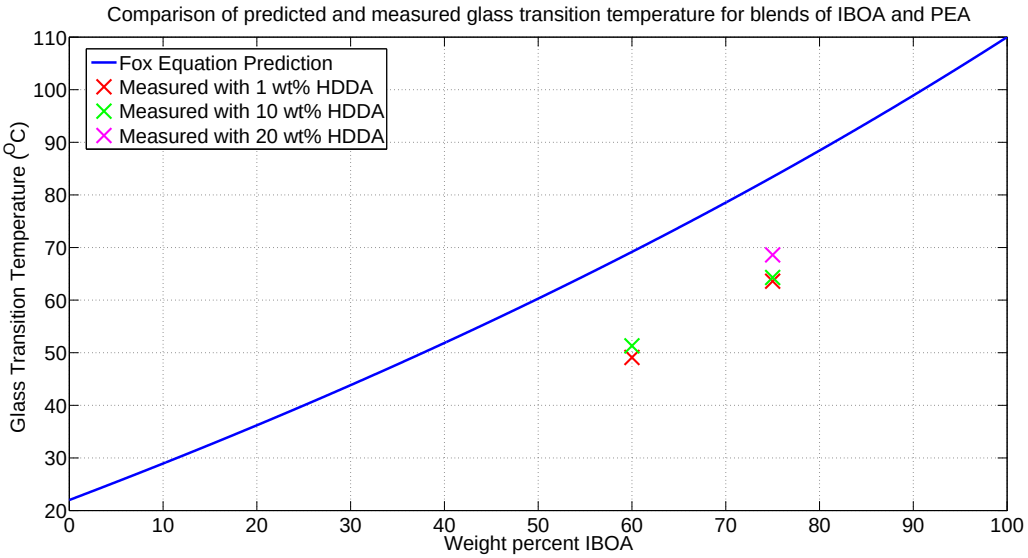

Figure 14: A comparison of the predicted and measured glass transition temperatures for varying copolymers and HDDA content.

For the 60 wt% case the measured T_g is 20.9^{o}C lower than the Fox Law predicts. A solution with 10 wt% HDDA was tested and showed a small increase in T_g as expected. Due to the T_g being lower than predicted, this copolymer was unsuitable as at room temperature it was in its transition region. A 75 wt% IBOA blend was then tried which gave a T_g of 64^{o}C. This mix was deemed acceptable for determining whether capsule survivability could be increased by using a shell with a suitable glass transition temperature. Preheating capsules made from this material to 50^{o}C before mixing would place them in the ductile and tough transition region, while at room temperature they are brittle. Solutions with 10 and 20 wt% HDDA were tested and the glass transition temperature was again seen to rise. Included for reference are graphs showing the modulus at 20^{o}C for the solutions tested, Figure 15.

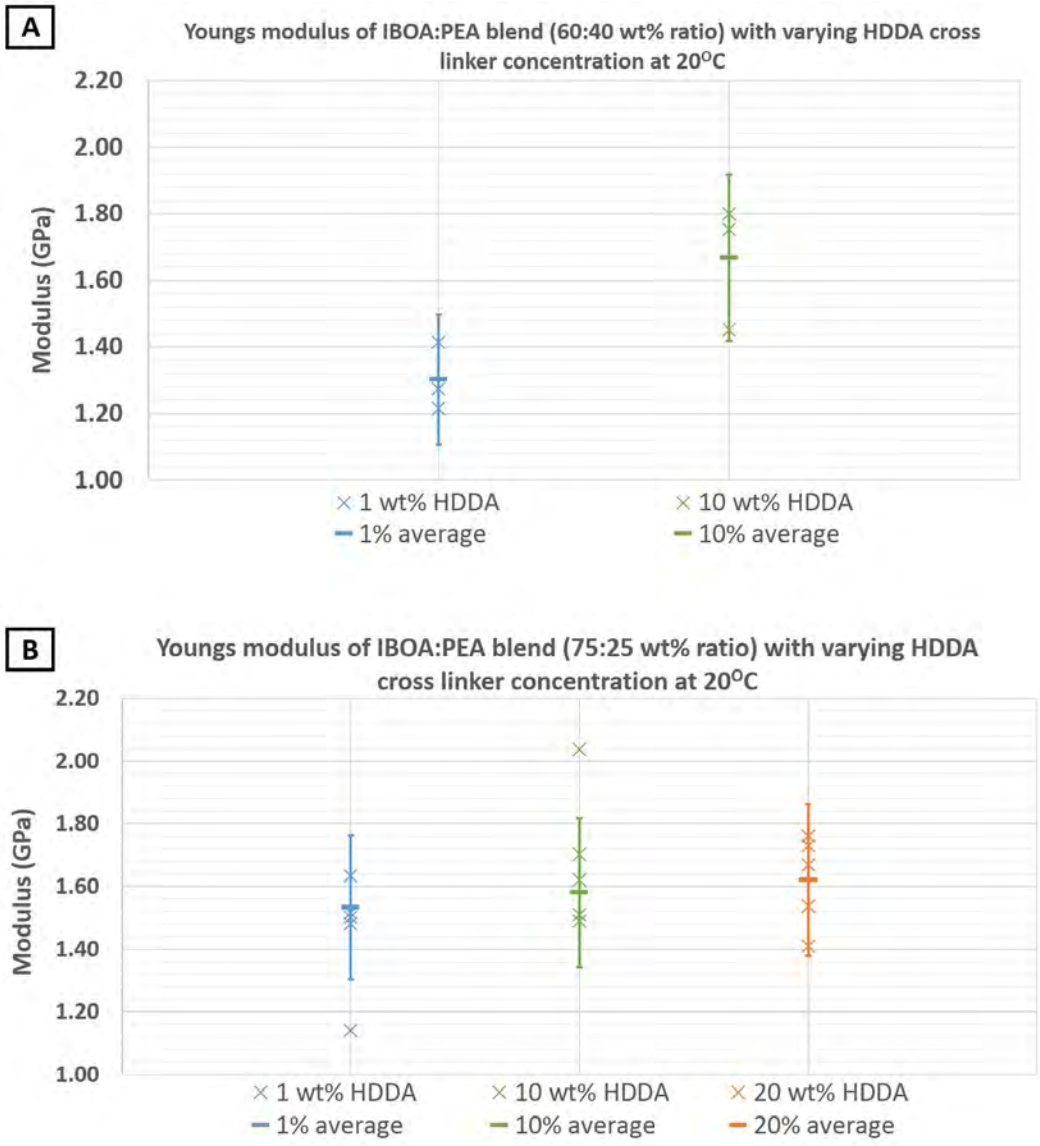

Figure 15: The Youngs modulus at 20^{o}C of blends of IBOA and PEA with varying amounts of HDDA. A) 60:40 wt%. B) 75:25 wt% IBOA:PEA. Error bars represent the propagated error in measuring the sample dimensions.

Polymerisation of the monomer leads to volume shrinkage due to the conversion of Van der Waals interactions to covalent bonds. The resulting internal stress lead to dimensional changes and potentially fracture [Moeck et al., 2014]. Shrinkage should be minimised for producing microcapsules due to their thin shell. Shrinkage values for IBOA and HDDA are 5.5% and 14% [Moeck et al., 2014]. Data for PEA could not be found, however, it is a monofunctional acrylate (as is IBOA) and these typically have smaller shrinkage values than multifunctional acrylates (HDDA). Hence, to minimise shrinkage while maintaining the reduction in porosity, 1 wt% HDDA should be used. The standard solution to be used for generating the capsules would be 75:25 wt% IBOA:PEA with 1 wt% HDDA and 2 wt% Darocur 1173 added.

4.2.4 The effect of BisGMA and Span 85

Later in the project, the shell material was changed by addition of the viscous acrylate BisGMA and the surfactant Span 85, the reasoning for this will be explained in section 4.3. The results of DMA tests on the new solutions are shown in Table 1.

Table 1: The effect of Span 85 and BisGMA on the modulus and glass transition temperature of the standard solution, where the standard solution is: 75:25 wt% IBOA:PEA with 1 wt% HDDA and 2wt% Darocur 1173 added.

Solution	**T_g (^{o}C)**	**E at 20^{o}C (GPa)**
Standard	64	1.5
Standard + 4wt% Span 85	52	1.1
70:30 wt% Standard:BisGMA	92	1.8
70:30 wt% Standard:BisGMA + 4wt% Span 85	81	1.4

Additionally, the modulus-temperature curve of one sample from each group is plotted in Figure 16. Addition of BisGMA clearly increased both the modulus and T_g while Span 85 has the opposite effect. Span 85 also has the effect of giving less distinction between the glassy and transition regions. The final solution used in production of microcapsules was 70:30 wt% Standard:BisGMA + 4wt% Span 85, fracture of these samples at 20^{o}C showed brittle behaviour, and the modulus-temperature curve suggests the mixing behaviour would be similar to the standard solution.

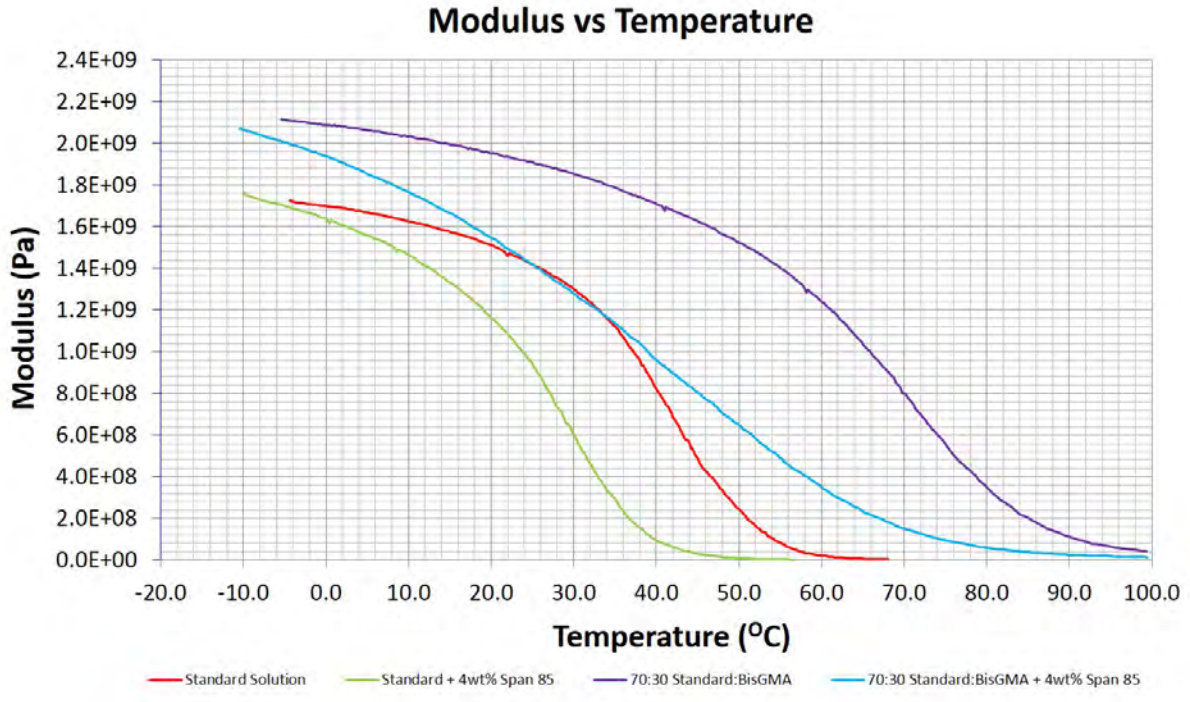

Figure 16: A representative curve for each of the modulus against temperature relationship of the 4 solutions used during microfluidic testing.

4.3 Microfluidics

4.3.1 Initial Testing

Using syringe pumps with the chip was highly unstable, the inner and outer PVA solutions would often connect, preventing formation of droplets, Figure 17.

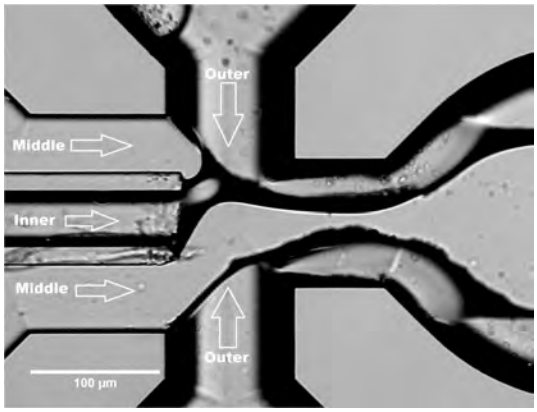

Figure 17: Image of the original microfluidic chip junction when used with syringe pumps.

Several factors contributed to this instability, firstly, syringe pump flow rates pulsate [Wehking et al., 2014]. Secondly, the microfluidic chip had been used prior to these experiments and the hydrophobic and hydrophilic surface coatings had become less effective, resulting in incorrect wetting of fluids. Finally, fibres had become lodged in the chip, disturbing flow profiles. The instability was removed by increasing the middle flow and reducing the outer and inner. Doing this however, prevented the break up of the middle fluid, resulting in single emulsions of water in oil (W/O). To overcome this 4 wt% of the surfactant Span 85 was added to the middle fluid, however, break up was still not achieved. Next 30 wt% Bisphenol A Glycidyl Methacrylate (BisGMA) was added to the middle solution, this is a highly viscous (7000000 cPs compared to IBOA at 10 cPs) UV curable acrylate. It was hoped that this would enable the middle flow rate to be reduced and facilitate break up, while still preventing the inner and outer connecting. This was again unsuccessful.

The change in material did, however, lead to an interesting observation. Before addition of BisGMA, the oil solution was less dense than water, hence the W/O emulsion formed a layer on top of water in the collection beaker. DMA results suggest the polymerised material should be stiff at room temperature. However, polymerisation gave a highly flexible foam, suggesting incomplete polymerisation, most likely due to oxygen inhibition at the surface. When BisGMA was added, the density increased causing the W/O emulsion to sink, producing a stiff foam when polymerised. The successful polymerisation, when submerged, shows that the effect of oxygen inhibition is reduced underwater, confirming the statement made by Studer et al. [2003].

Using pressure pumps, stable flow was achieved and double emulsions formed, however, they either contained several cores or gave a random distribution of droplet sizes and thicknesses, Figure 18.

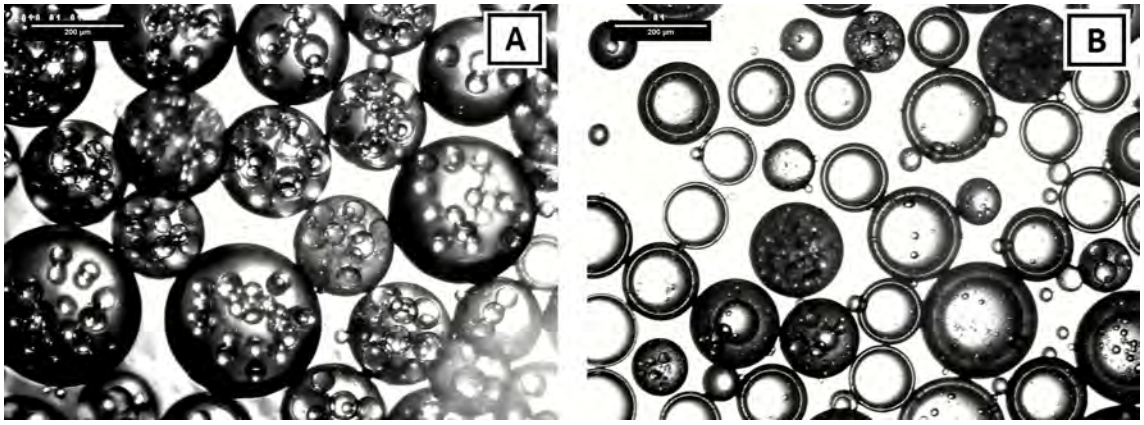

Figure 18: Double emulsions formed using the original chip and pressure pumps. A) Multicores at flow rates of 5 : 2.4 : 93 μl/min inner : middle : outer. B) Predominantly single core at 6.55 : 2.79 : 77 μl/min.

A new microfluidic chip was then deployed due to a blockage in the original. Figure 19 shows a typical image of the junction in the new chip when producing droplets.

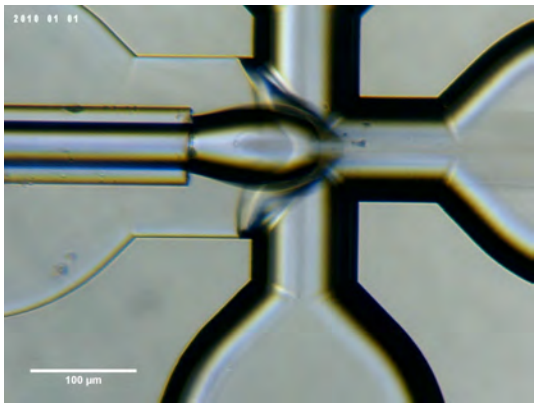

Figure 19: New microfluidic chip junction when used with pressure pumps showing flow conditions required for stable double droplet formation.

The flow is more uniform in the new chip and the surfaces are correctly wetted i.e. there is no oil on the outer channel surface as there was in the old chip, helping confirm the surface treatments in the old chip had deteriorated. This was further backed up by the reduction in pressure required to drive flows in the new chip. For example, an outer flow rate of 77 μl/min required a pressure of 371 mbar in the new chip compared to 1100 mbar in the old chip. Using the new chip and the pressure pumps, monodisperse double emulsion droplets were formed using the standard solution with BisGMA and Span 85 added. It was decided to use this solution rather than the standard solution as Span 85 aided droplet break up and BisGMA ensured droplets sank preventing oxygen inhibition of floating droplets.

4.3.2 Outer Flow Rate

Testing capsules with varying diameters and shell wall thickness to identify an optimum geometry for maximising the self-healing efficiency is a very interesting area. To do this, it is necessary to be able to produce capsules with varying geometries. Figure 20 shows the effect of outer flow rate on the measured internal and outer diameter of the produced double emulsions and the subsequent shell wall thickness. It is believed that this data was collected in the dripping regime, however, the capturing rate of the microscope was not high enough to confirm this.

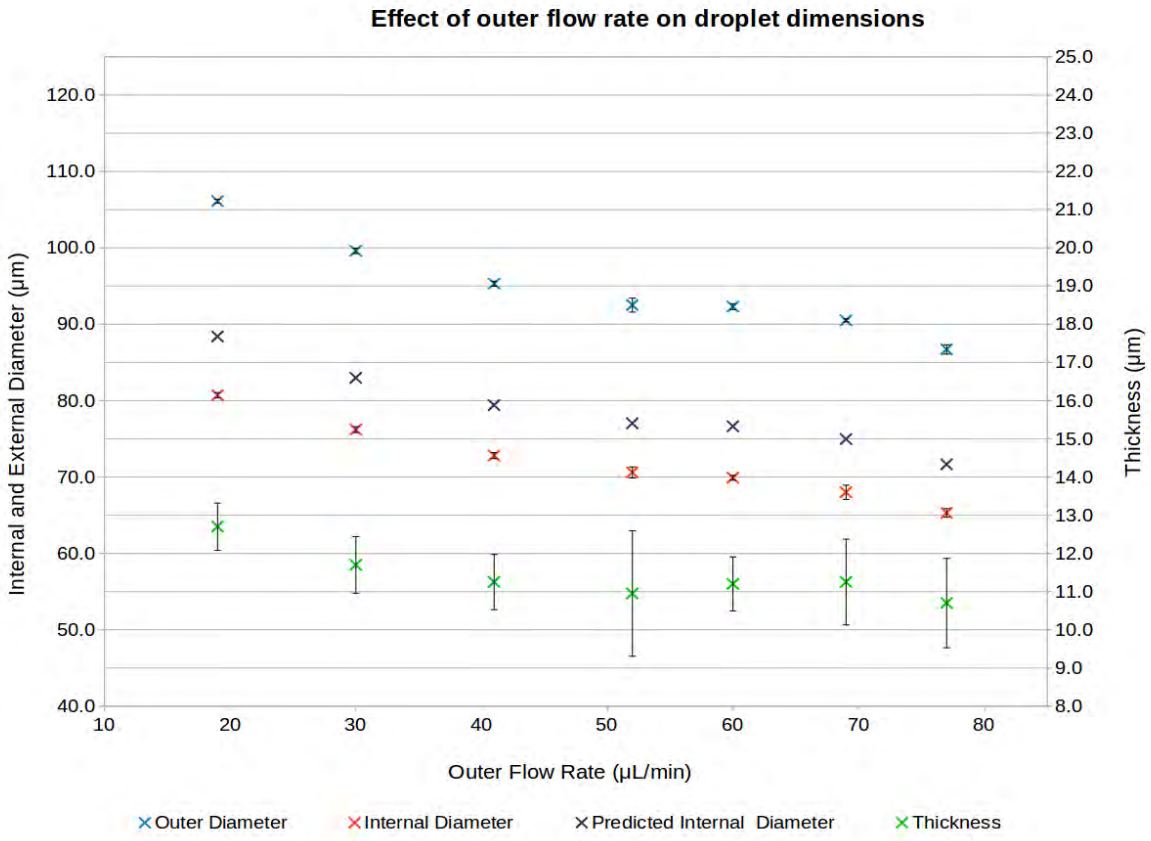

Figure 20: Data points for the effect of outer flow rate on the inner and outer diameter of the droplets. Inner and middle flow rates held constant under pressure control at 2.09 and 1.55 μl/min respectively during data collection. Plotted on the secondary Y axis is the measured thickness.

Increasing the outer flow rate decreases both the outer and inner diameter, with a total decrease in outer diameter of 19.4 μm over the range of outer flows measured. A small decrease in shell wall thickness is noted, however this effect is smaller than that on the outer diameter, particularly given the error in the readings. This suggests that the outer flow rate predominantly controls the outer diameter of the capsule; in agreement with [Chen et al., 2011, Nie et al., 2005]. Further reduction in the outer flow rate resulted in flow instability and no droplet production.

Also plotted is the predicted internal diameter. This was calculated by assuming that the ratio of the volumetric inner and outer flow rates must equal the volume ratio of inner and outer material due to mass conservation, hence:

$$\frac{Q_i}{Qm} = \frac{\frac{4}{3}\pi\frac{D_i^3}{8}}{\frac{4}{3}\pi\frac{D_o^3}{8} - \frac{4}{3}\pi\frac{D_i^3}{8}} \tag{4}$$

where Q_i and Q_m are the inner and middle volumetric flow rates, D_i the internal diameter to be calculated and D_o the measured external diameter. Hence, the predicted internal diameter is given by:

$$D_i = D_o\sqrt[3]{\frac{Q_i}{Q_m + Q_i}} \tag{5}$$

The predicted inner diameter is consistently larger than measured and hence the predicted thickness is always smaller than measured, varying between 29 and 31%. The consistency in the difference suggests the error is systematic. Initially it was suspected the difference was due to the focus point used in the microscopy. The images were taken at the focus corresponding to the sharpest distinction between the core and shell, this may not, however, correspond to the centreline of the sphere. However, calculating the focus position required for the predicted thickness to be 30% less than the measured, gives a deviation from the centreline of 27.7μm (64% of the outer radius). The large deviation makes this explanation seem unlikely. Reading the literature on the subject identified that this problem has been attributed to the different refractive indices of the core and shell [Chen et al., 2014].

Additionally, it was noticed that fewer secondary sized droplets were produced when the outer flow rate was reduced, Figure 21.

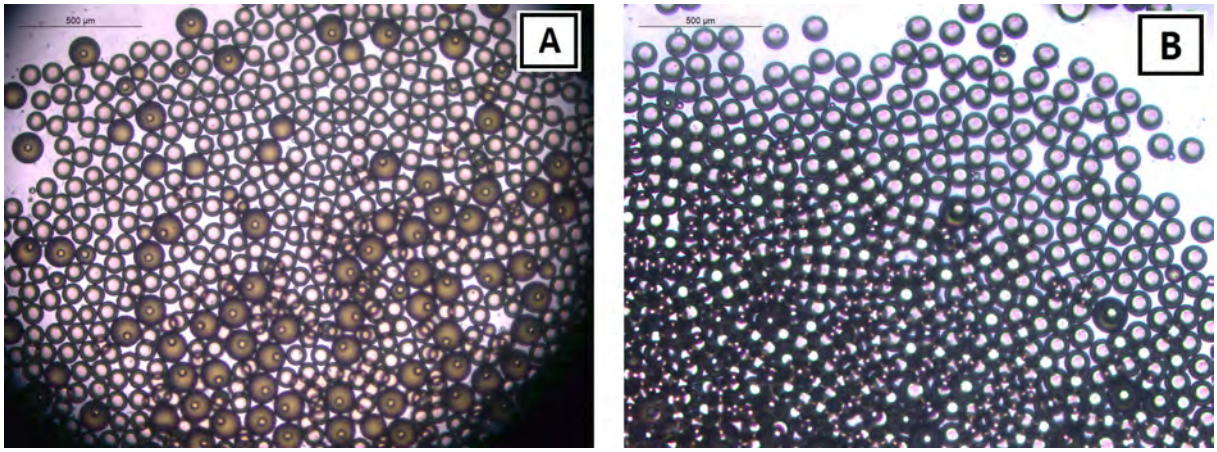

Figure 21: Droplets produced with an outer flow rate of A) 84 μl/min. B) 19 μl/min.

A possible explanation is that the increased outer flow causes some jetting of the flow, and hence formation of more secondary droplets. Operating at lower outer flow rates gives greater efficiency in the use of the shell material, however, the greatest efficiency occurred at flow rates just above the instability limit.

4.3.3 Inner Flow Rate

Figure 22 shows the effect of the inner flow on droplet dimensions.

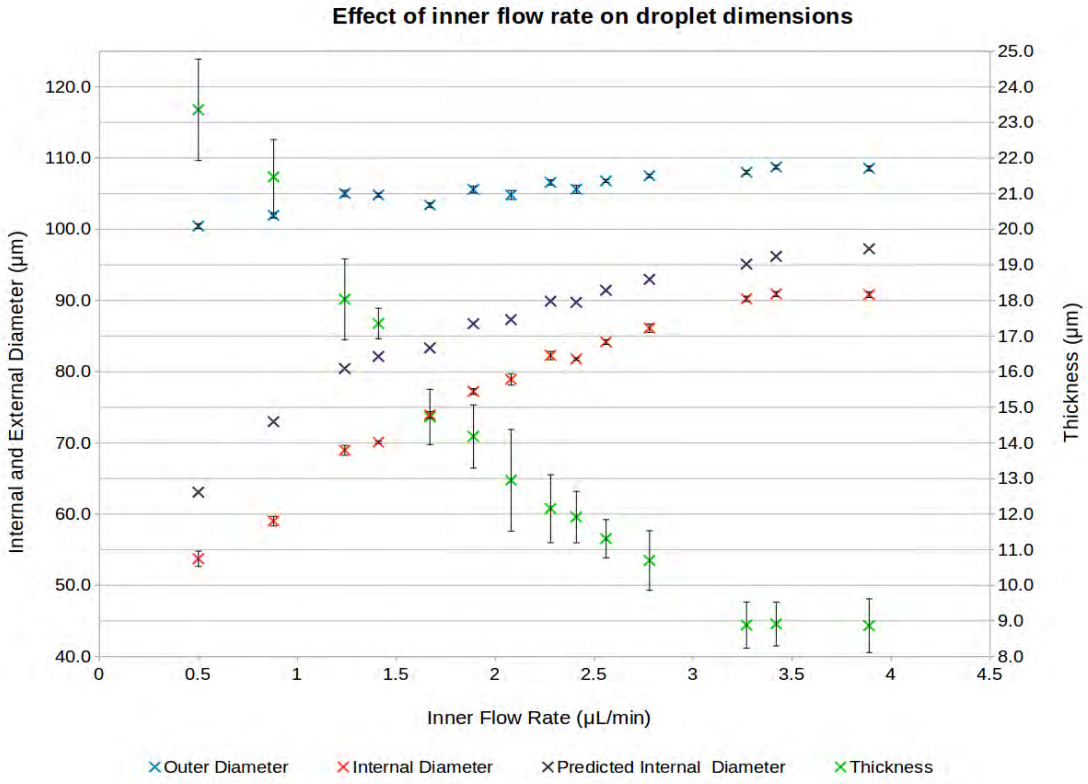

Figure 22: Data points for the effect of inner flow rate on the inner and outer diameter of the droplets. Outer and middle flow rates held fixed under flow control at 20 and 1.52 μl/min. Plotted on the secondary Y axis is the measured thickness.

Increasing inner flow gives a small increase in outer diameter (8.1 μm over the measured range) but a much larger increase in internal diameter (37.1 μm), giving a decrease in measured thickness of 14.5 μm. Again, the predicted thickness was calculated to be an average of 31% smaller than the measured, further suggesting a systematic error.

Both Chen et al. [2011] and Nie et al. [2005] found a slight decrease in outer diameter with increasing inner flow, compared to the slight increase found here. Internal diameter behaviour was similar in all cases. In both referenced studies, middle phases of significantly lower viscosities were used. Seo et al. [2005] demonstrated that when producing single emulsions, inner phases of high viscosity (>586 cPs) displayed different droplet size

dependencies to low viscosity (<14 cPs) fluids. While this study cannot be directly applied to double emulsions, it suggests that the higher viscosity solution may be the cause of the difference.

The decrease in thickness appears to reach a plateau for inner flow rates above 3 μl/min, for flow rates above 4 μl/min the system became unstable suggesting that the minimum achievable thickness was reached. Thinner shells may be producible by varying the middle and outer flow rates as well, however, this requires further investigation. Chen et al. [2011] produced capsules with a minimum achievable thickness of 7-10 μ, shell thinner than this ruptured in the high shear environment. If the predicted thickness is assumed to be the actual thickness, then shells of 5.7 μm were produced indicating that the higher viscosity middle fluid used in this project is able to withstand greater shear forces and produce thinner shells.

This investigation has shown that the dimensions of the capsules are controllable by the inner and outer fluid flows. To complete the relationships, the effect of the middle fluid flow rate would need to be investigated, as unfortunately due to time considerations this was not possible.

4.4 Micocapsule Production

When droplets were polymerised by UV exposure, non-uniformity was observed in the shell wall compared to the un-polymerised state, Figures 23 and 24.

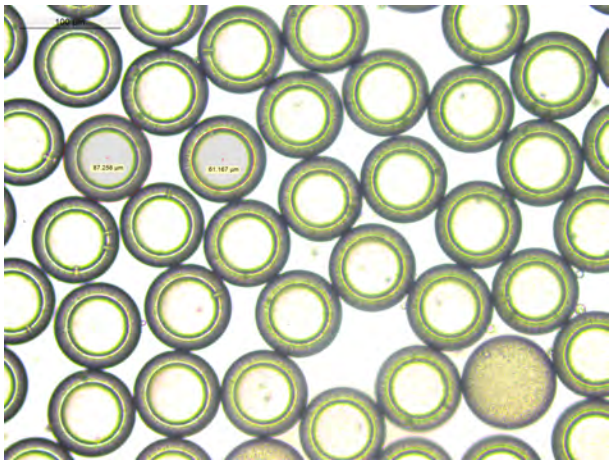

Figure 23: Droplets before polymerisation. Capsule size indicated.

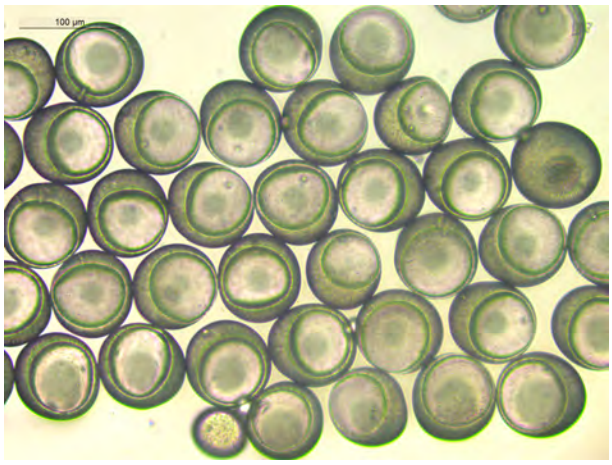

Figure 24: Capsules immediately after 300 seconds polymerisation using a UV lamp.

Shell material was redistributed around the capsule, giving regions of solid shell as thick as 20 μm and as thin as 1 μm, from the initially uniform 12 μm thick liquid shell. The most likely cause of this non uniformity is the difference in density between the core (1.00 g/ml) and the shell fluid (1.05 g/ml). The difference in density causes the shell to sink relative to the core, forming an inhomogeneous shell thickness [Datta et al., 2014]. Additionally, it was suspected that the UV exposure set up used accentuated the effect, due to the uneven UV exposure (irradiated only from below) and the relatively slow cure offered by the low intensity lamp used. The Sylvania BL350 intensity is 0.03 W/cm^2 compared to the Omnicure S1000 used by Chen et al. [2011] at 18 W/cm^2. It is believed that the region of the capsule closest to the UV lamp, which will be the thickest due to the density difference, has the fastest cure rate. As the material begins to polymerise in this region, the process draws molecular chains into the region from surrounding areas, binding to the forming chains. If the cure was fast, the time for this to occur before other regions began to cure would be very small and this effect would be reduced. However, due to the low intensity lamp, the cure time is long enough to allow diffusion and generate non uniform thickness. Moeck et al. [2014] supports this hypothesis stating that curing at high UV intensities gives a faster cure, with less diffusion-controlled addition.

The polymerised capsules from Figure 24 were left to dry on the microscope slide and observed, after 15 minutes further deformation could be seen, Figure 25. Additionally, what is believed to be the lightly stained PVA core material was seen flowing between the capsules.

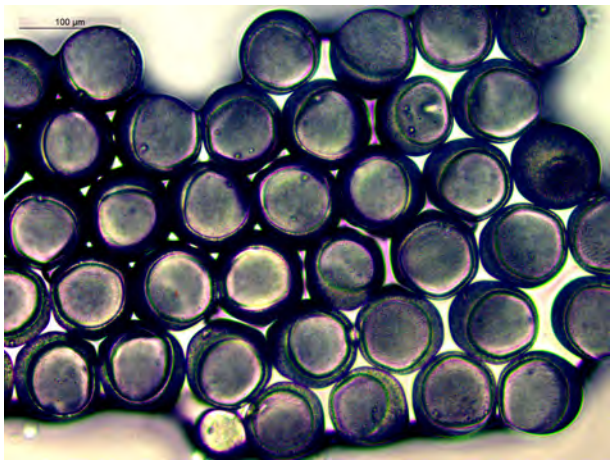

Figure 25: Capsules 15 minutes after polymerisation. PVA flows identifiable by light pink regions between capsules. Image colour saturation adjusted to aid visualisation.

While a specific capsule could not be identified as the source of the fluid, it is strongly suspected that buckling of the capsule shell wall led to fracture and release of the core. The cause of buckling is a capillary pressure difference established across the shell, greater externally. This occurs as the PVA outer solution evaporates leaving menisci in the pores of the polymer shell. Abbaspourrad et al. [2013] state that this capillary pressure would be given by:

$$P_c = \frac{2\gamma}{r_p} \tag{6}$$

Where γ is the surface tension between the outer fluid and air (44.7 mN/m for PVA) and r_p the average radius of a pore in the polymer shell (approximately 10 nm), giving a capillary pressure of 9 MPa.

For the shell to buckle, the capillary pressure must exceed the threshold buckling pressure of a thin walled spherical shell given by, [Datta et al., 2014]

$$P_b = \frac{2E}{\sqrt{3(1-\nu^2)}} \left(\frac{t}{R_o}\right)^2 \tag{7}$$

E was found during DMA analysis (E = 1.4 GPa) and ν can be taken to be 1/3, R_o is the capsule radius and t the wall thickness. For the case of a uniform wall thickness of 12 μm the buckling threshold is 130 MPa, so no buckling would occur if polymerisation

resulted in a uniform wall thickness. For a non uniform wall thickness t becomes the thickness at the thinnest point, optical images give this as 1 μm. Hence, the buckling threshold is 1 MPa, indicating buckling will occur as observed. This effect places a minimum wall thickness on uniform capsules which when using 2 wt% PVA as the outer fluid is given by $0.07R_o$, 3.2 μm for the radius of capsules analysed here.

To see if more uniform UV exposure improved polymerisation, an aluminium foil reflector was placed above the petri-disk, resulting in the polymerised capsules seen in Figure 26.

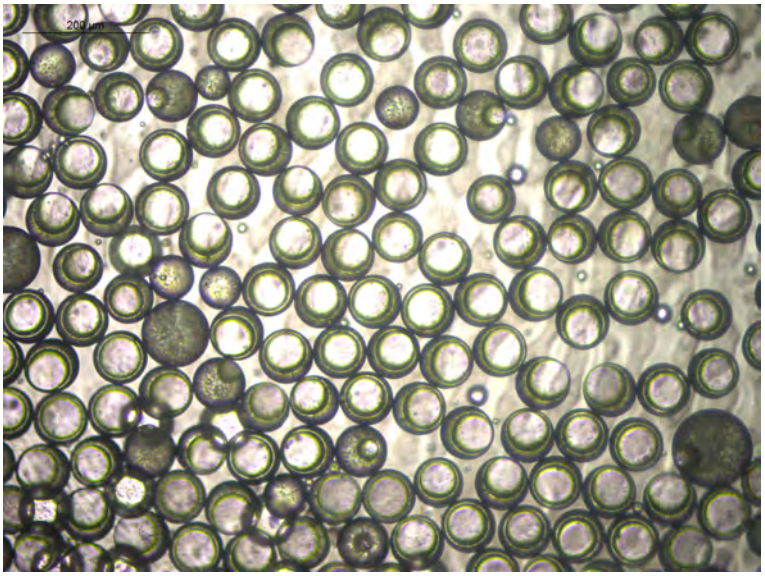

Figure 26: Capsules immediately after 300 seconds polymerisation in a container covered with aluminium foil to reflect the UV light.

While many capsules still displayed non uniformities, some capsules polymerised with a more uniform shell thickness. This shows some improvement over the original set-up with further improvements potentially possible using lamps above and below the sample. However, the predominant issue is sinking of the denser shell relative to the core material. Datta et al. [2014] capsules polymerised within 15 minutes of formation did not buckle, whereas, those polymerised after did. Hence, reducing the time before polymerisation by polymerising the droplets continuously as they leave the device 'in-situ', may solve the problem. A possible further refinement to the polymerisation uniformity is increased photoinitiator concentration, while 2 wt% was found to be most effective in the bulk samples, the thinner microcapsules may benefit from a higher concentration. This would allow faster polymerisation and, due to the thin shell, the curing of sub surface material would not be affected as greatly as in thicker samples.

The capsules polymerised using the reflector were imaged with a Scanning Electron Microscope (SEM). Two sizes of capsule were visible corresponding to the primary and secondary droplets produced in the microfluidic chip, Figure 27.

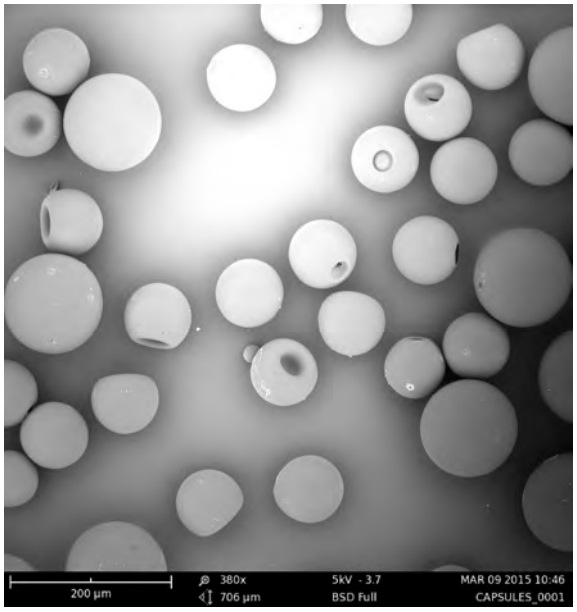

Figure 27: Polymerised capsules viewed by SEM after vacuum drying for 48 hours.

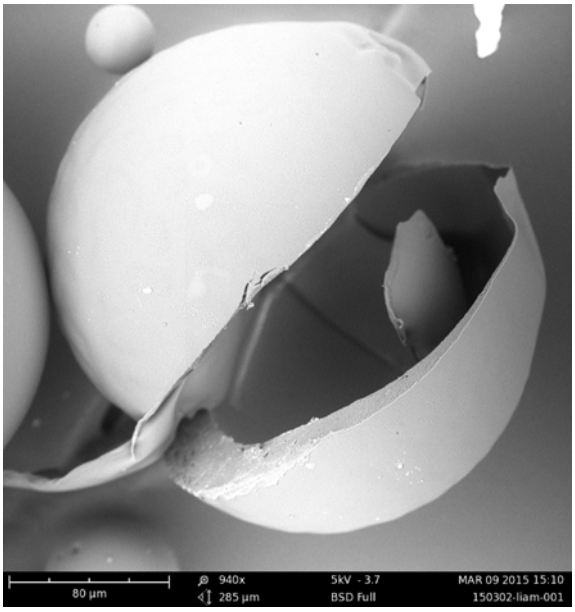

Figure 28: SEM image of individual capsule cut with a scalpel.

Deformation was observed in the majority of the primary capsules, while the larger, thicker shelled and unwanted secondary capsules appeared uniform and un-deformed. This corresponds well with the proposed cause of buckling deformation. To investigate the wall thickness, a scalpel was used to slice capsules, Figure 28. The shell wall thickness is as expected from the optical images, tapering from a maximum of 31 μm to a minimum of 1 μm. In the larger secondary capsules, shell wall thickness inhomogeneities were also present, however, the thicker wall prevents buckling.

Capsule failure occurs by an inward buckling of the capsule wall at its thinnest region followed by rupture, Figure 29A, supporting the proposed method of deformation.

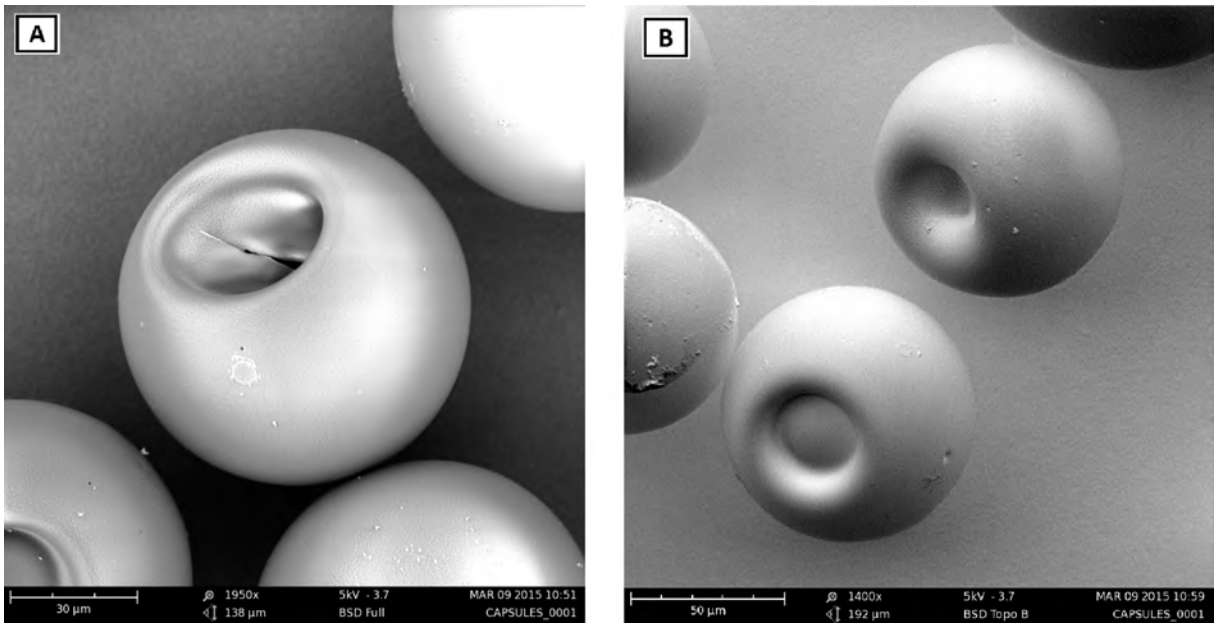

Figure 29: SEM image of capsules. A) Buckling leading to fracture. B) Buckled but intact.

The capsules that survived also displayed an inward deformation, Figure 29B, indicating that rupture occurs after the deformation and not vice versa. A capsule is more likely to rupture as the wall thickness of the thinnest region decreases, suggesting capsules polymerised shortly after formation are more likely to survive. Additionally, if a capsule contains an air bubble in the thin region of the shell, this will act as a stress concentration and make failure more likely.

4.5 Thermogravimetric Analysis

The results of thermogravimetric analysis on a sample of polymerised capsules and a sample of the polymerised capsule material can be used to evaluate the water content of the capsules. The capsule material does not show any significant mass loss until approximately 240^{o}C, Figure 30.

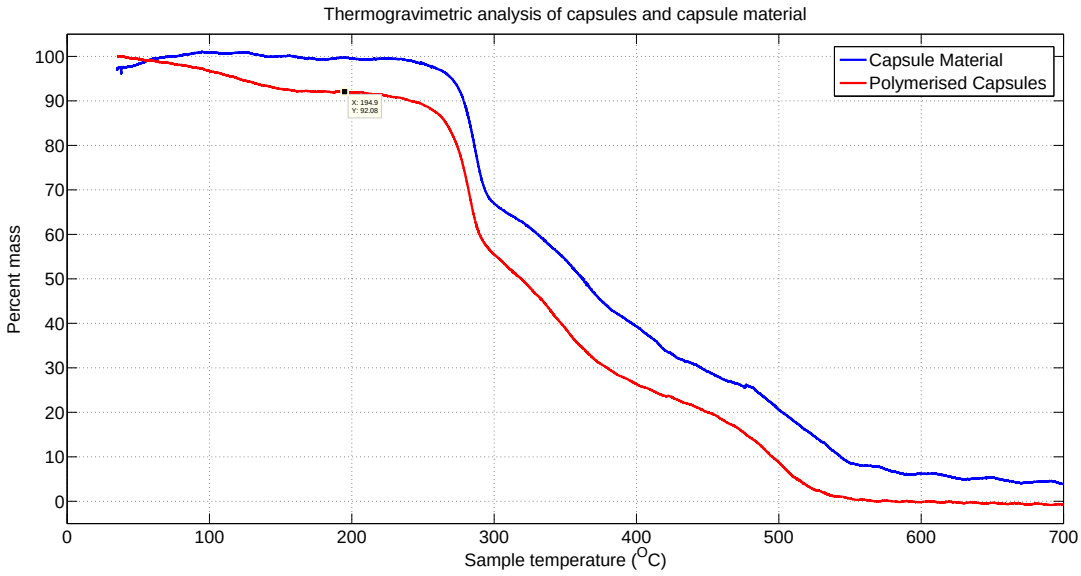

Figure 30: Thermogravimetric analysis of a sample of vacuum dried capsules and a sample of the capsule shell material showing percentage of the initial test mass remaining with temperature. The point indicated was used to calculate the water content of the capsules.

It can, therefore, be assumed that any mass loss in the capsules at temperatures lower than this is due to water loss. The capsule sample loses weight up to approximately 160^{o}C where the weight loss plateaus until 240^{o}C, from here it begins to resemble the capsule material curve. Taking the point indicated, on the plateau at 194.9^{o}C, will give an estimate of the water loss. This point gives a water loss and hence water content percentage of 7.92%. For the capsules tested (internal diameter - 61.8 μm, external - 87.1 μm) the expected water mass content percentage is 33.6% assuming all the capsules are intact. Hence, the percentage of intact capsules after polymerisation is 24% assuming all water loss was from the core.

4.6 Cement Paste Prisms

As this is a completely new area of research, it was decided that despite the non uniform polymerisation process, it would be worthwhile casting cement paste samples to observe the capsule behaviour in response to mixing, binding and fracture. It was decided not to investigate the effect of preheating the capsules on their survivability. A number of factors contributed to this decision. Firstly, as the new shell material had, at this stage, not been characterised with the DMA it could not be known if the desired increase in ductility and fracture toughness would occur. Secondly, due to the low rate of capsule production (approximately 1g/hour) only small cement samples could be used and so hand mixing of the cement was required, reducing the likelihood of breakage. Finally, the cement paste contained no large aggregates which could cause impact damage to the capsules. Should the specimen size be scaled up and be used with an aggregate mix, the survivability of the capsules is likely to be reduced.

After the cement paste and capsules were mixed and moulded, a small sample of the mix was observed under the microscope, Figure 31.

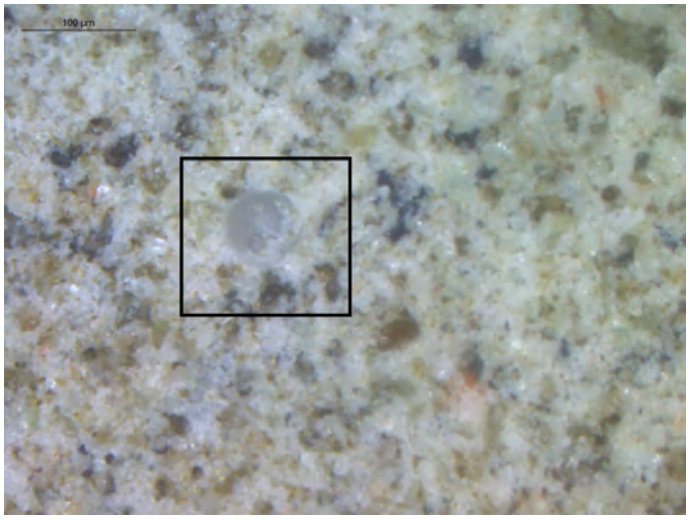

Figure 31: Cement paste after mixing. Capsule identified.

This technique was used by Wang et al. [2014] to assess if capsules had survived by identifying the objects in the mix with a capsule like appearance. During observation, capsules could be identified in the mix, however, it could not be determined if these were intact capsules or if the capsules had sustained damage during the mixing. Additionally, any capsules which are fragmented into small pieces will be hard to detect. A simple improvement, that would however, be limited to identifying only intact capsules, would be the inclusion of fluorescence dye in the core material. Hence, any intact capsules would be visible using fluorescence microscopy. Inclusion of fluorescence dye in the shell material, may additionally allow for the detection of broken capsule fragments.

A sample which was broken immediately after de-moulding was observed with the SEM. This revealed that the cement paste had not strongly bound to the capsules, Figures 32 and 33. Capsules were not fractured during the fracture of the cement prism and instead either remained embedded in the fracture surface or were pulled out leaving a crater.

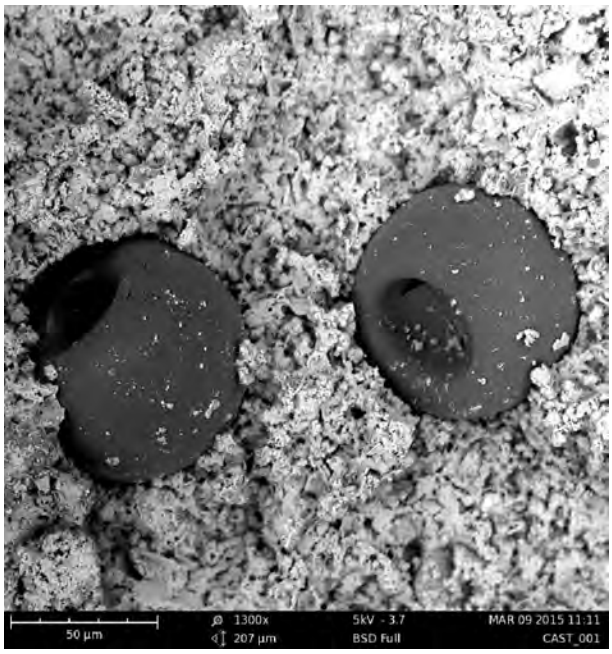

Figure 32: SEM image of damaged capsules in the fracture surface of a sample broken immediately after de-moulding.

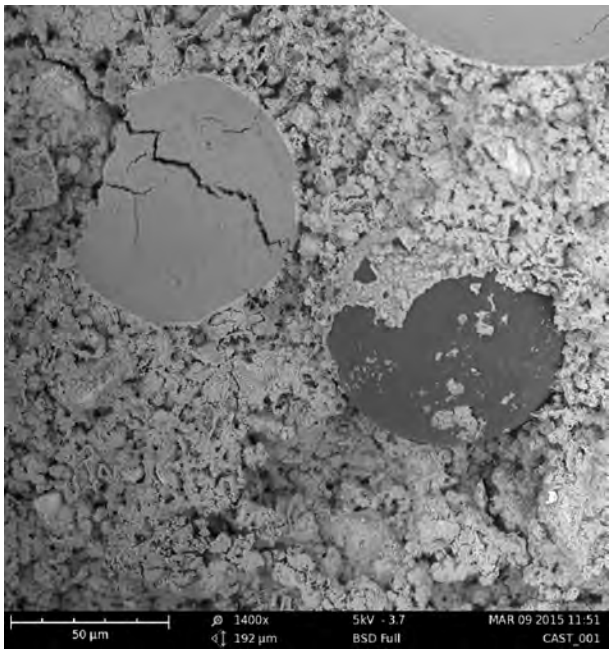

Figure 33: SEM image of a remaining capsule and crater. Sample was broken immediately after de-moulding.

The absence of cement from the capsule depressions, Figure 32 left hand capsule, suggests the buckling deformation has taken place some time after the cement has begun to cure. The capsules placed in these samples were stored underwater the whole time from polymerisation to casting, hence, were not exposed to the external capillary pressure caused by drying. During cement curing, water will be removed from the capsule surroundings, this will lead to the generation of the capillary pressure as in drying and lead to the buckling of the shell. The fact that the capsule is still able to deform in this way shows that the cement has not bound to the capsule.

Additional samples were placed under water for continued hydration. As well as strengthening the cement, it was hoped this would increase the bond strength between the cement and the capsules. A sample was removed, dried and fractured after 3 days before imaging with the SEM, Figures 34 and 35.

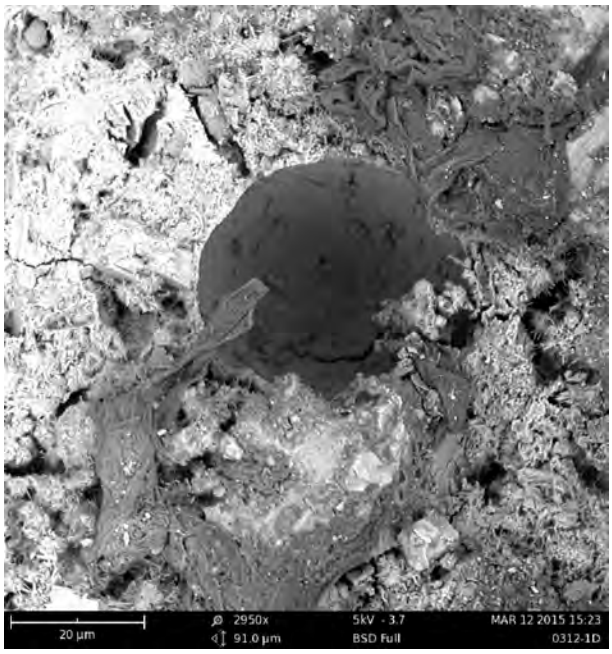

Figure 34: Material believed to be red stained PVA flowing out of a capsule crater. Sample broken after 3 days hydration.

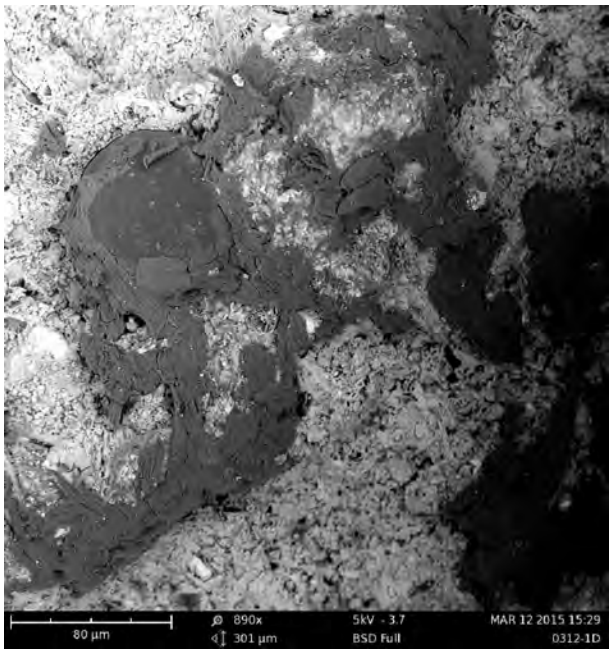

Figure 35: SEM image of the fracture surface of a sample hydrated for 3 days showing material flowing from a capsule.

What appeared to be a polymeric material was visible, surrounding some capsules and craters. The structure of the deposition suggested the capsule core fluid had flown out off and away from the capsules before solidifying. The core material of the capsules is a PVA solution stained with red food colouring, as the water in the solution evaporates it will leave behind the PVA which will form a polymeric glue when dried. While the PVA is used to ease the generation of double emulsion droplets, and not as a healing agent, it has had the unexpected benefit of enabling the identification of core material release from the capsules. No PVA was identified in locations far from either a capsule or a crater.

Figure 34 shows the appearance of the majority of the locations from which material had flown. The remains of the capsules cannot be seen, suggesting the binding of the capsules to the cement is not sufficiently strong for the capsule to remain inside the sample when placed under vacuum. This suggests that the capsule fractures due to shear deformation, leading to sliding of the fracture surfaces over each other or compression, causing crushing of the capsules. Tensile fracture of the capsules seems unlikely as the bonding does not seem sufficiently strong for the capsules to fracture in preference to a crack propagating around the capsule cement interface. Figure 35 shows PVA flows around a remaining capsule, it is assumed that this capsule sustained sufficient damage

to release the core contents but not such that it was dislodged from its place or broken into small pieces. It was noted that the majority of the released PVA was found in one half of the sample, this would suggest it was located in the compressive side of the prism when broken in bending. As no PVA was identified in the sample broken immediately after de-moulding, it is believed that PVA released by capsules broken during curing is diluted by the remaining water and able to flow over a much larger area and is hence, not deposited in concentrated amounts.

Interesting features were also observable under the optical microscope, several traces of orange material were seen, Figure 36.

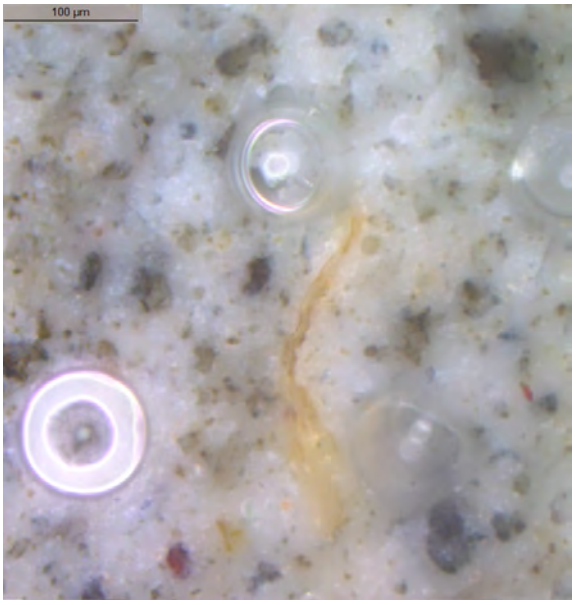

Figure 36: The fracture surface of a sample hydrated for 3 days, showing a flow of orange material believed to be red stained PVA.

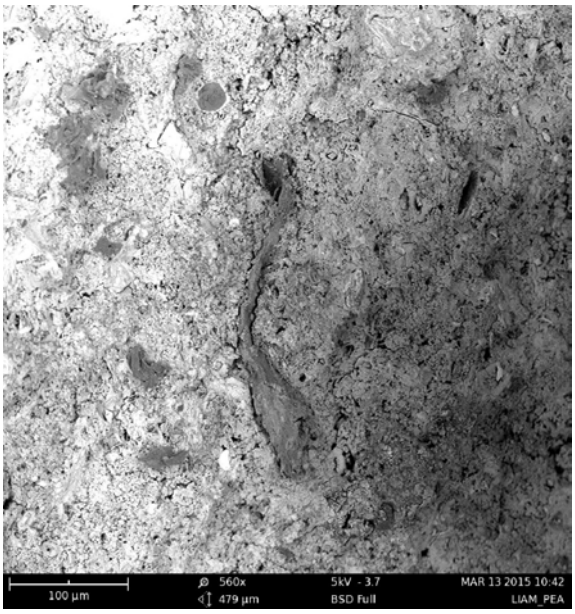

Figure 37: The same region of the fracture surface viewed under SEM showing the same pattern of material.

The orange colour of the trace suggested it could be the PVA core material due to the use of red food colouring to stain it. Recording the location of the feature on the sample enabled the same location to be found in the SEM, Figure 37. The PVA flow is clearly visible in the SEM image and corresponds to the orange trace in the optical image, not all the PVA deposits were as easily visible under the optical microscope however. The use of a fluorescence dye would be a sensible improvement for optical detection, enabling both easier detection and greater differentiation from cement hydration products. Surprisingly the 4 reflective circular objects visible optically, which were initially thought to be microcapsules, are absent from the SEM image. The sample was then gold coated and viewed again, gold coating can aid the viewing of non-conductive samples. This did not reveal any further detail. The origin of these optical features is unknown but has implications for identifying microcapsules optically. Using fluorescence dye would distinguish capsules and these features.

Control samples containing no capsules were also produced for comparison. A sample, hydrated for 3 days, fractured and viewed optically, displayed the optical features, Figure 38, previously seen in Figure 36.

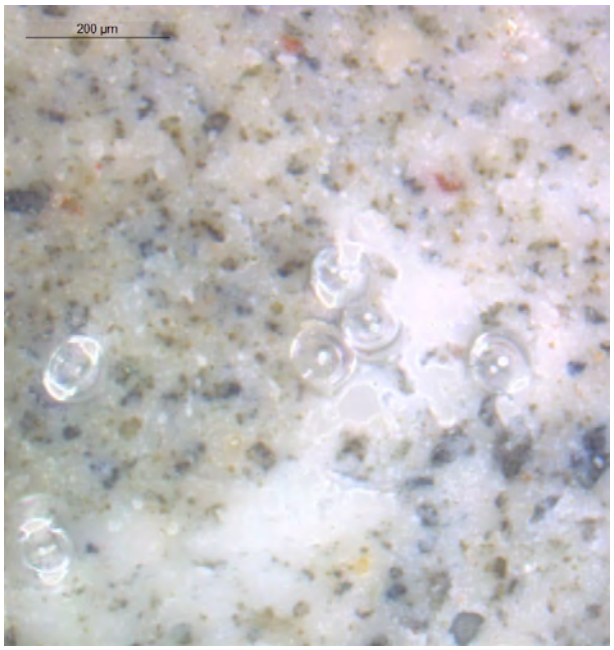

Figure 38: Optical microscope image of a control sample containing no capsules. Visible are optical features similar to a microcapsule.

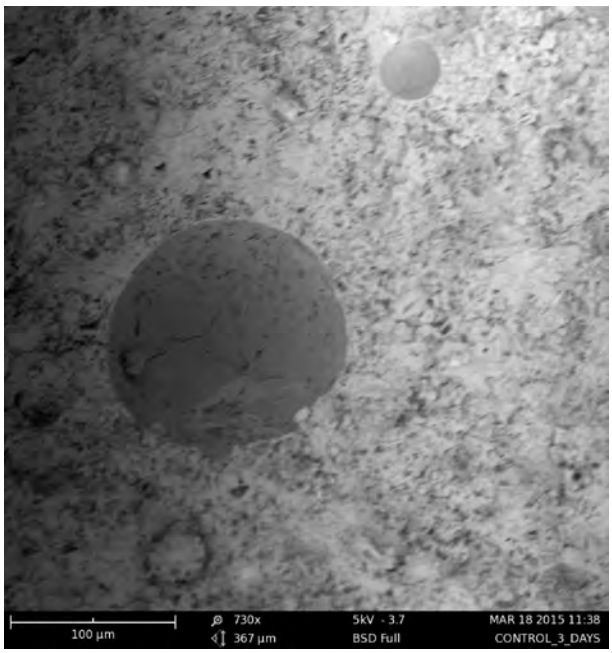

Figure 39: SEM image of the control sample showing craters with approximately the same diameter as a microcapsule.

This confirms that the objects cannot be microcapsules. SEM images again did not display these features, suggesting they are the result of an optical phenomenon. SEM images did however, reveal a small number of craters, some with a similar diameter to the microcapsules and some smaller (40 μm), Figure 39. These are expected to be due to air trapped in the cement paste during moulding, and may be mistaken for capsule craters.

To help confirm that the polymeric material identified previously was PVA, 1ml of PVA solution was placed onto a piece of the 3 day hydrated control sample and left to dry. Optical and SEM images were taken, Figures 40 and 41.

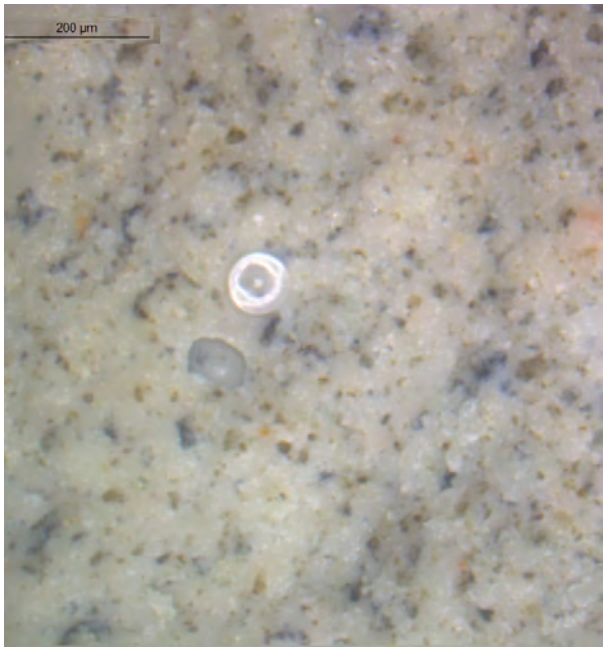

Figure 40: Optical image of PVA coated control sample.

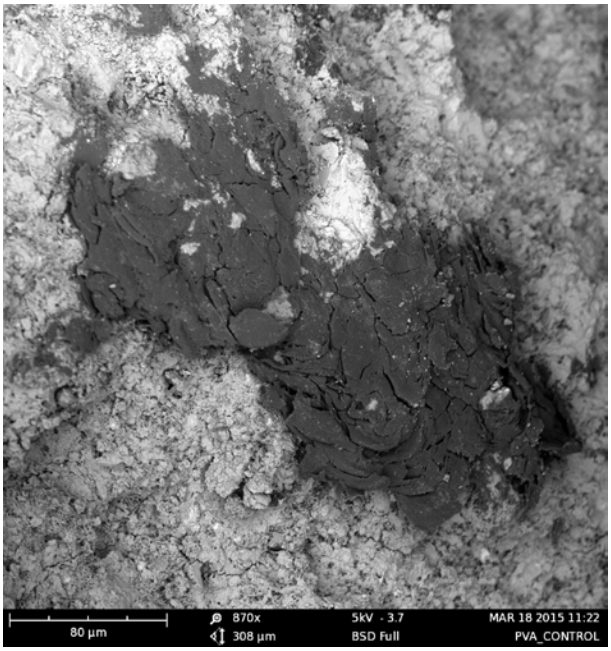

Figure 41: SEM image of PVA coated control sample showing a region covered in dried PVA

Optically small orange regions were visible and SEM images showed large quantities of material, with a very similar appearance to that seen in the capsule samples, deposited over the sample. From this it was concluded that the material seen was PVA from the core of the capsules.

5 Conclusions

5.1 Main Findings

A summary of the main findings from this project follows.

- The thermo-mechanical properties of both individual acrylate polymers, PEA and IBOA, and their copolymers were measured using Dynamic mechanical analysis.
- The effect of BisGMA and Span 85 on the thermo-mechanical properties was also quantified. BisGMA increased both the modulus and glass transition temperature while Span 85 decreased both.
- Stable double emulsion droplets were formed using the commercial Dolomite Microfluidics double emulsion chip. Droplets were on the order of 100 μm outer diameter and 10 μm thickness.
- The shell thickness and outer diameter of formed droplets was found to be controllable using the flow rates. Increased outer flow rate predominantly led to a decreased outer diameter, with a small decrease in thickness. Additionally lower outer flow rates gave fever unwanted secondary droplets, thereby increasing the efficiency of the system. Increased inner flow rate led to a small increase in outer diameter and a large decrease in thickness down to a plateau suggesting a minimum achievable shell thickness.
- Droplets were polymerised by UV exposure resulting in an inhomogeneous shell wall thickness and damaged capsules indicating improvements are required in the polymerisation set up. Thermogravimetric analysis was used to quantify the number of intact capsules after polymerisation.
- Capsules cast in cement paste showed weak capsule-cement bonding, resulting in pull out rather than fracture of the capsule.
- In cement hydrated for 3 days, capsule core material was seen to have flown from capsules upon fracture of the sample. Imaging of the fracture surface suggested compressive strain resulted in capsule fracture while tensile strain still resulted in capsule pull out.

In conclusion, it has been shown that it is possible to manufacture polymer shell microcapsules containing a liquid core using microfluidics and cast them inside small cement paste specimens. Fracture of the capsules has been demonstrated in compressive

deformation and suspected in shear, however, not in tensile. Should a healing agent be encapsulated within the shell, the demonstrated fracture may facilitate self-healing behaviour. This research area is still very much in its infancy and further work is required to refine the methods used and establish the feasibility for capsule fracture due to tensile cracks in construction materials.

5.2 Future Work

Achieving a stronger bond between the capsule and the cement would be the next stage of further investigation. A possible way of achieving this, whilst maintaining the same shell material, is the inclusion of nano or microparticles in the shell. Chen et al. [2011] showed it was possible to include silica nano particles, either on the outer surface or homogeneously dispersed through the shell of microfluidically produced acrylate microcapsules. These nanoparticles are prohibitively expensive (£97.3/g Sigma-Aldrich). However, an alternative may be the use of silica fume, of a fine enough grade with particle sizes on the order of a micron. Silica fume is extensively used in high performance concretes, [Diamond and Sahu, 2006]. It is, therefore, proposed that if microcapsules were made with silica fume particles protruding from the shell, the bond strength would be increased by favourable interaction with the matrix. Additionally, the surface roughness would increase, potentially facilitating stronger bonding. Chen noted that inclusion of nanoparticles embrittled the capsules, which could be favourable as it would increase the probability of a crack fracturing the capsule.

To truly evaluate the self healing potential, it is necessary to show encapsulation of a healing agent in the core is possible. Candidates for encapsulation would be sodium silicate or two part adhesives among others [Van Tittelboom and De Belie, 2013]. Single component adhesives such as cyanoacrylate would cure in the chip due to contact with the other fluids making them unsuitable for this application. Two part adhesives would not have this issue and could either be encapsulated in separate capsules, or in separate cores of the same capsule, [Lee et al., 2014], which may improve mixing post release.

Investigating the effect of capsule geometry and proportion on the self-healing efficiency and effect on initial mechanical properties of the cement or concrete will also be required to achieve optimum conditions. Fine tuning of the capsules' geometry is achievable using the flow rates, however should larger differences in capsule outer diameter be required for investigation, it would require using a chip with different geometry at the junction [Chen et al., 2011].

Achieving capsule production scale up (from the low production rates of 1g/hour) will be of fundamental importance to allowing both testing in larger cement samples and

eventually full scale structures. A simple way to scale up production is the use of multiple chips, this however requires the purchase of three pressure pumps per chip and is hence, not economically viable. Romanowsky et al. [2012] designed a high throughput double emulsion generator by producing 15 droplet generators on the same chip requiring only one set of pumps. This achieved a production rate of 42g/hour and the design could easily be extended to include many more junctions on a single chip. Designing and producing a suitable chip using Romanowsky's methods is likely to be required as research progresses.

Investigating different shell materials is an alternative avenue. This could include looking at shell materials which polymerise in ways other than UV exposure, for example, silicon shelled capsules produced by [Vilanova et al., 2013]. Or even investigating the possibility of shells which release the core due to the chemical environment. The steel reinforcement in concrete corrodes due to chloride ions, which can diffuse through the concrete. A shell which reacts to chloride ions and releases a chloride ion neutraliser could be utilised to reduce the reinforcement corrosion rate.

6 Acknowledgements

I would like to thank Professor Abir Al-Tabbaa and Dr Antonis Kanellopoulos for their supervision and guidance throughout the project. Additionally, I would like to thank Lívia Souza for her help and advice with the experimental techniques used during the project.

7 Bibliography

A. Abbaspourrad, W. J. Duncanson, N. Lebedeva, S.-H. Kim, A. P. Zhushma, S. S. Datta, P. A. Dayton, S. S. Sheiko, M. Rubinstein, and D. A. Weitz. Microfluidic fabrication of stable gas-filled microcapsules for acoustic contrast enhancement. *Langmuir*, 29(40): 12352–12357, 2013.

V. D. Athawale and M. A. Kulkarni. Preparation and properties of urethane/acrylate composite by emulsion polymerization technique. *Progress in Organic Coatings*, 65(3): 392–400, 2009.

H. F. Chan, Y. Zhang, Y.-P. Ho, Y.-L. Chiu, Y. Jung, and K. W. Leong. Rapid formation of multicellular spheroids in double-emulsion droplets with controllable microenvironment. *Scientific reports*, 3, 2013.

D. Chattopadhyay, S. S. Panda, and K. Raju. Thermal and mechanical properties of

epoxy acrylate/methacrylates uv cured coatings. *Progress in Organic Coatings*, 54(1): 10–19, 2005.

P. W. Chen, R. M. Erb, and A. R. Studart. Designer polymer-based microcapsules made using microfluidics. *Langmuir*, 28(1):144–152, 2011.

P. W. Chen, G. Cadisch, and A. R. Studart. Encapsulation of aliphatic amines using microfluidics. *Langmuir*, 30(9):2346–2350, 2014.

C. Cramer, P. Fischer, and E. J. Windhab. Drop formation in a co-flowing ambient fluid. *Chemical Engineering Science*, 59(15):3045–3058, 2004.

S. S. Datta, A. Abbaspourrad, E. Amstad, J. Fan, S.-H. Kim, M. Romanowsky, H. C. Shum, B. Sun, A. S. Utada, M. Windbergs, et al. 25th anniversary article: double emulsion templated solid microcapsules: mechanics and controlled release. *Advanced Materials*, 26(14):2205–2218, 2014.

M. De Rooij and E. Schlangen. Self-healing phenomena in cement-based materials. *Draft of State-of-the-Art report of RILEM Technical Committee*, 2011.

S. Diamond and S. Sahu. Densified silica fume: particle sizes and dispersion in concrete. *Materials and structures*, 39(9):849–859, 2006.

Dolomite Microfluidics. Double emulsion system notes. http://www.dolomite-microfluidics.com/images/stories/PDFs/application_notes/double_emulsion_system_application_note.pdf, 2010.

C. Dry. Matrix cracking repair and filling using active and passive modes for smart timed release of chemicals from fibers into cement matrices. *Smart Materials and Structures*, 3(2):118, 1994a.

C. M. Dry. Smart multiphase composite materials that repair themselves by a release of liquids that become solids. In *1994 North American Conference on Smart Structures and Materials*, pages 62–70. International Society for Optics and Photonics, 1994b.

T. G. Fox. Influence of diluent and of copolymer composition on the glass temperature of a polymer system. *Bull Am Phys Soc*, 1(123):22060–6218, 1956.

P. Glöckner. *Radiation Curing: Coatings and Printing Inks ; Technical Basics, Applications and Trouble Shooting*. American coatings literature. Vincentz Network, 2008. ISBN 9783866309074.

B. Hilloulin, K. Van Tittelboom, E. Gruyaert, N. De Belie, and A. Loukili. Design of polymeric capsules for self-healing concrete. *Cement and Concrete Composites*, 55: 298–307, 2015.

Y. Hu, D. Pine, and L. G. Leal. Drop deformation, breakup, and coalescence with compatibilizer. *Physics of Fluids (1994-present)*, 12(3):484–489, 2000.

C. Joseph, A. Jefferson, B. Isaacs, R. Lark, and D. Gardner. Experimental investigation of adhesive-based self-healing of cementitious materials. *Magazine of Concrete Research*, 62(11):831–843, 2010.

I. Kaltzakorta, E. Erkizia, M. De, and G. Berriozabal. Cement derivative with self-sealing capacity, Aug. 21 2013. URL `http://www.google.com/patents/EP2628716A1?cl=en`. EP Patent App. EP20,100,858,353.

J. M. Lankveld and J. Lyklema. Adsorption of polyvinyl alcohol on the paraffin—water interface. i. interfacial tension as a function of time and concentration. *Journal of Colloid and Interface Science*, 41(3):454–465, 1972.

J.-C. Lee and M. H. Litt. Glass transition temperature-composition relationship of oxyethylene copolymers with chloromethyl/(ethylthio) methyl, chloromethyl/(ethylsulfinyl) methyl, or chloromethyl/(ethylsulfonyl) methyl side groups. *Polymer journal*, 32(3):228–233, 2000.

S. S. Lee, A. Abbaspourrad, and S.-H. Kim. Nonspherical double emulsions with multiple distinct cores enveloped by ultrathin shells. *ACS applied materials & interfaces*, 6(2): 1294–1300, 2014.

M. d. C. López-García, D. Beebe, and W. Crone. Characterization of poly (isobornyl acrylate) as a construction material for microfluidic applications. *Journal of applied polymer science*, 105(4):1894–1902, 2007.

C. Meyer. Concrete materials and sustainable development in the USA. *Structural engineering international*, 14(3):203–207, 2004.

H. Mihashi, Y. KANEKO, T. Nishiwaki, and K. Otsuka. Fundamental study on development of intelligent concrete characterized by self-healing capability for strength. *Transactions of the Japan Concrete Institute*, 22:441–450, 2001.

A. Moeck, R. Bianchi, V. Petry, R. Weder, and D. Helsby. Shrinkage of uv oligomers and monomers. http://radtech.org/2014proceedings/papers/technical-conference/Formulation, 2014.

Z. Nie, S. Xu, M. Seo, P. C. Lewis, and E. Kumacheva. Polymer particles with various shapes and morphologies produced in continuous microfluidic reactors. *Journal of the American chemical society*, 127(22):8058–8063, 2005.

J. Nunes, S. Tsai, J. Wan, and H. Stone. Dripping and jetting in microfluidic multiphase flows applied to particle and fibre synthesis. *Journal of physics D: Applied physics*, 46 (11):114002, 2013.

L. Peng, M. Yang, S.-s. Guo, W. Liu, and X.-z. Zhao. The effect of interfacial tension on droplet formation in flow-focusing microfluidic device. *Biomedical microdevices*, 13(3): 559–564, 2011.

M. B. Romanowsky, A. R. Abate, A. Rotem, C. Holtze, and D. A. Weitz. High throughput production of single core double emulsions in a parallelized microfluidic device. *Lab on a chip*, 12(4):802–807, 2012.

M. Seo, Z. Nie, S. Xu, M. Mok, P. C. Lewis, R. Graham, and E. Kumacheva. Continuous microfluidic reactors for polymer particles. *Langmuir*, 21(25):11614–11622, 2005.

T. M. Squires and S. R. Quake. Microfluidics: Fluid physics at the nanoliter scale. *Reviews of modern physics*, 77(3):977, 2005.

K. Studer, C. Decker, E. Beck, and R. Schwalm. Overcoming oxygen inhibition in uv-curing of acrylate coatings by carbon dioxide inerting, part i. *Progress in Organic Coatings*, 48(1):92–100, 2003.

D. V. Val and M. G. Stewart. Life-cycle cost analysis of reinforced concrete structures in marine environments. *Structural safety*, 25(4):343–362, 2003.

S. Van der Zwaag. Routes and mechanisms towards self healing behaviour in engineering materials. *Bulletin of the Polish Academy of Sciences: Technical Sciences*, 58(2):227–236, 2010.

K. Van Tittelboom and N. De Belie. Self-healing in cementitious materials—a review. *Materials*, 6(6):2182–2217, 2013.

N. Vilanova, C. Rodriguez-Abreu, A. Fernandez-Nieves, and C. Solans. Fabrication of novel silicone capsules with tunable mechanical properties by microfluidic techniques. *ACS applied materials & interfaces*, 5(11):5247–5252, 2013.

J. Wang, H. Soens, W. Verstraete, and N. De Belie. Self-healing concrete by use of microencapsulated bacterial spores. *Cement and Concrete Research*, 56:139–152, 2014.

X. Wang, F. Xing, M. Zhang, N. Han, and Z. Qian. Experimental study on cementitious composites embedded with organic microcapsules. *Materials*, 6(9):4064–4081, 2013.

J. D. Wehking, M. Gabany, L. Chew, and R. Kumar. Effects of viscosity, interfacial tension, and flow geometry on droplet formation in a microfluidic t-junction. *Microfluidics and nanofluidics*, 16(3):441–453, 2014.

Z. Wicks, F. Jones, S. Pappas, and D. Wicks. *Organic Coatings: Science and Technology*. Wiley, 2007. ISBN 9780470079065. URL https://books.google.co.uk/books?id=KEU0yixqUTYC.

J. Woudhuysen. *Why is construction so backward*. Wiley-Academy, Chichester Hoboken, NJ, 2004. ISBN 0470852895.

Y. Yang, E.-H. Yang, and V. C. Li. Autogenous healing of engineered cementitious composites at early age. *Cement and concrete research*, 41(2):176–183, 2011.

A Appendix

A.1 Risk Assessment Retrospective

The risk assessment completed before practical project work was undertaken accurately described the risks associated with production of the capsules using microfluidics, polymerisation and general handling of chemicals. Unexpected risks were, however, encountered during the project work, these were:

- RSI while making the moulds for bulk samples. As around 50 individual moulds had to be made, the process proved to be relatively straining on the elbows. Adequate breaks were, however, taken to reduce the risk.
- Use of liquid nitrogen during DMA testing to cool samples. The lab technician filled the dewar flash container and his advice on subsequent handling was followed.

A.2 Microfluidic Flow Rates

Outer

Flow Rates (ul/min)			Pressure (mbar)			Diameter (µm)				
						Measured				Predicted
Inner	Middle	Outer	Inner	Middle	Outer	Outer	SD	Internal	SD	Internal
1.97	1.52	77	300	380	371	86.7	0.61	65.3	0.56	71.7
2.00	1.52	69	300	380	330	90.5	0.19	68	0.93	75.0
2.06	1.54	60	300	380	290	92.3	0.39	69.9	0.32	76.6
2.13	1.56	52	300	380	250	92.5	0.92	70.6	0.72	77.0
2.14	1.56	41	300	380	200	95.3	0.33	72.8	0.40	79.4
2.15	1.57	30	300	380	150	99.6	0.35	76.2	0.39	83.0
2.18	1.59	19	300	380	100	106.1	0.27	80.7	0.35	88.4

Inner

Flow Rates (ul/min)			Pressure (mbar)			Diameter (µm)				
						Measured				Predicted
Inner	Middle	Outer	Inner	Middle	Outer	Outer	SD	Internal	SD	Internal
3.89	1.52	20	490	384	100	108.5	0.35	90.8	0.40	97.2
3.42	1.52	20	440	385	100	108.7	0.28	90.9	0.34	96.2
3.27	1.52	20	420	380	100	108.0	0.27	90.2	0.38	95.1
2.78	1.52	20	400	381	100	107.5	0.24	86.1	0.59	93.0
2.56	1.52	20	380	381	100	106.8	0.20	84.2	0.34	91.4
2.41	1.52	20	360	380	99	105.6	0.55	81.8	0.17	89.7
2.28	1.52	19	300	400	100	106.6	0.37	82.3	0.59	89.9
2.08	1.52	20	280	390	99	104.8	0.63	78.9	0.80	87.3
1.89	1.52	20	260	388	98	105.6	0.48	77.2	0.41	86.7
1.67	1.52	20	240	416	95	103.4	0.31	73.9	0.46	83.3
1.41	1.52	20	220	458	95	104.8	0.27	70.1	0.16	82.1
1.24	1.52	20	200	392	93	105.0	0.43	69.0	0.70	80.4
0.88	1.52	20	170	391	93	101.9	0.38	59.0	0.67	73.0
0.50	1.52	20	170	375	93	100.4	0.35	53.7	1.08	63.1

Figure 42: Flow rates and pressures used during testing, with corresponding droplet dimensions. Predicted internal diameter also shown.